International Journal of Biological Macromolecules 194 (2022) 128–143

Contents lists available at ScienceDirect

International Journal of Biological Macromolecules

journal homepage: www.elsevier.com/locate/ijbiomac

Emergence of unique SARS-CoV-2 ORF10 variants and their impact on protein structure and function

Sk. Sarif Hassan [a,*], Kenneth Lundstrom [b], Ángel Serrano-Aroca [c], Parise Adadi [d], Alaa A. A. Aljabali [e], Elrashdy M. Redwan [f,t], Amos Lal [g], Ramesh Kandimalla [h,u], Tarek Mohamed Abd El-Aziz [i,v], Pabitra Pal Choudhury [j], Gajendra Kumar Azad [k], Samendra P. Sherchan [l], Gaurav Chauhan [m], Murtaza Tambuwala [n], Kazuo Takayama [o], Debmalya Barh [p,w], Giorgio Palu [q], Pallab Basu [r], Vladimir N. Uversky [s,*]

[a] Department of Mathematics, Pingla Thana Mahavidyalaya, Maligram, Paschim Medinipur 721140, West Bengal, India
[b] PanTherapeutics, Rte de Lavaux 49, CH1095 Lutry, Switzerland
[c] Biomaterials and Bioengineering Lab, Centro de Investigacion Traslacional San Alberto Magno, Universidad Catolica de Valencia San Vicente Martir, c/Guillem de Castro, 94, 46001 Valencia, Valencia, Spain
[d] Department of Food Science, University of Otago, Dunedin 9054, New Zealand
[e] Department of Pharmaceutics and Pharmaceutical Technology, Yarmouk University, Faculty of Pharmacy, Irbid 566, Jordan
[f] Biological Science Department, Faculty of Science, King Abdulaziz University, Jeddah, Saudi Arabia
[g] Department of Medicine, Division of Pulmonary and Critical Care Medicine, Mayo Clinic, Rochester, MN, USA
[h] Applied Biology, CSIR-Indian Institute of Chemical Technology, Uppal Road, Tarnaka, Hyderabad 500007, Telangana, India
[i] Department of Cellular and Integrative Physiology, University of Texas Health Science Center at San Antonio, 7703 Floyd Curl Dr, San Antonio, TX 78229-3900, USA
[j] Indian Statistical Institute, Applied Statistics Unit, 203 B T Road, Kolkata 700108, India
[k] Department of Zoology, Patna University, Patna, Bihar, India
[l] Department of Environmental Health Sciences, Tulane University, New Orleans, LA, 70112, USA
[m] School of Engineering and Sciences, Tecnologico de Monterrey, 64849 Monterrey, Nuevo Leon, Mexico
[n] School of Pharmacy and Pharmaceutical Science, Ulster University, Coleraine BT52 1SA, Northern Ireland, UK
[o] Center for iPS Cell Research and Application, Kyoto University, Kyoto 6068507, Japan
[p] Centre for Genomics and Applied Gene Technology, Institute of Integrative Omics and Applied Biotechnology (IIOAB), Nonakuri, Purba Medinipur 721172, West Bengal, India
[q] Department of Molecular Medicine, University of Padova, Via Gabelli 63, 35121 Padova, Italy
[r] School of Physics, University of the Witwatersrand, Johannesburg, Braamfontein 2000, 721140, South Africa
[s] Department of Molecular Medicine, Morsani College of Medicine, University of South Florida, Tampa, FL 33612, USA
[t] Therapeutic and Protective Proteins Laboratory, Protein Research Department, Genetic Engineering and Biotechnology Research Institute, City of Scientific Research and Technological Applications, New Borg EL-Arab 21934, Alexandria, Egypt
[u] Department of Biocemistry, Kakatiya Medical College, Warangal, Telangana, India
[v] Zoology Department, Faculty of Science, Minia University, El-Minia 61519, Egypt
[w] Department of Genetics, Ecology and Evolution, Institute of Biological Sciences, Federal University of Minas Gerais, Belo Horizonte 31270-901, Brazil

ARTICLE INFO

Keywords:
SARS-CoV-2
ORF10
Co-occurring mutations
Intrinsic protein disorder
And ubiquitin ligase complex

ABSTRACT

The devastating impact of the ongoing coronavirus disease 2019 (COVID-19) on public health, caused by the Severe Acute Respiratory Syndrome Coronavirus 2 (SARS-CoV-2) has made targeting the COVID-19 pandemic a top priority in medical research and pharmaceutical development. Surveillance of SARS-CoV-2 mutations is essential for the comprehension of SARS-CoV-2 variant diversity and their impact on virulence and pathogenicity. The SARS-CoV-2 open reading frame 10 (ORF10) protein interacts with multiple human proteins CUL2, ELOB, ELOC, MAP7D1, PPT1, RBX1, THTPA, TIMM8B, and ZYG11B expressed in lung tissue. Mutations and co-occurring mutations in the emerging SARS-CoV-2 ORF10 variants are expected to impact the severity of the virus and its associated consequences. In this article, we highlight 128 single mutations and 35 co-occurring mutations

* Corresponding authors.
E-mail addresses: sksarifhassan@pinglacollege.ac.in (Sk.S. Hassan), angel.serrano@ucv.es (Á. Serrano-Aroca), alaaj@yu.edu.jo (A.A.A. Aljabali), lradwan@kau.edu.sa (E.M. Redwan), mohamedt1@uthscsa.edu (T.M.A. El-Aziz), pabitrapalchoudhury@gmail.com (P. Pal Choudhury), gkazad@patnauniversity.ac.in (G.K. Azad), sshercha@tulane.edu (S.P. Sherchan), gchauhan@tec.mx (G. Chauhan), m.tambuwala@ulster.ac.uk (M. Tambuwala), kazuo.takayama@cira.kyoto-u.ac.jp (K. Takayama), dr.barh@gmail.com (D. Barh), giorgio.palu@unipd.it (G. Palu), pallabbasu@gmail.com (P. Basu), vuversky@usf.edu (V.N. Uversky).

https://doi.org/10.1016/j.ijbiomac.2021.11.151
Received 25 September 2021; Received in revised form 18 November 2021; Accepted 22 November 2021
Available online 2 December 2021

in the unique SARS-CoV-2 ORF10 variants. The possible predicted effects of these mutations and co-occurring mutations on the secondary structure of ORF10 variants and host protein interactomes are presented. The findings highlight the possible effects of mutations and co-occurring mutations on the emerging 140 ORF10 unique variants from secondary structure and intrinsic protein disorder perspectives.

1. Introduction

Severe Acute Respiratory Syndrome Coronavirus 2 (SARS-CoV-2) continues the pandemic spread of coronavirus disease 2019 (COVID-19), with over 227 million people confirmed infected and at least 4.66 million deaths worldwide [1,2]. In 2021, in almost every region of the SARS-CoV-2 genome, several mutations compared to the wild-type SARS-CoV-2 (NC 045512) were discovered [3–5]. Like other RNA viruses, the SARS-CoV-2 is constantly evolving by mutations and new variants with different characteristics are emerging [6–12]. Detection and mutation surveillance of SARS-CoV-2 is of utmost priority to investigate the origin and to combat the virus [13]. To date, no method can rapidly diagnose multiple viral infections and determine variants in a high-throughput manner [14]. SARS-CoV-2 is one of the largest RNA viruses with a genome of approximately 29Kb, which includes eleven open reading frames (ORFs) [15–18]. These ORFs (1a and 1b) possess two polypeptides that are translated into sixteen non-structural proteins (NSP1–16) [19–21]. The main non-structural proteins (NSP) include RNA-dependent RNA polymerase (RdRp or NSP12) and a 3′-5′ exonuclease [22]. RNA viruses typically show a high mutation rate ranging from 10^{-6} to 10^{-4} [23,24]. Notably, SARS-CoV-2 possesses the 3′-5′ exonuclease capable of correcting mistakes during replication [25]. While surveilling mutations to comprehend the genetic diversity across various SARS-CoV-2 variants, it is also important to decipher whether the increase in mutation frequency is because of the natural selection, and to determine the possible consequences for SARS-CoV-2 fitness, such as increased infectivity and pathogenicity, or due to adaptation, thereby becoming drug-resistant or possessing ability to evade the immune system [26,27]. Non-synonymous mutations of various SARS-CoV-2 proteins have been reported [28–31].

The ORF proteins are dispensable for viral growth *in vitro*, and might play important roles within the environment of the infected host [32]. The SARS-CoV-2 open reading frame 10 (ORF10) protein shows no sequence similarity with other known coronavirus proteins [33,34]. The SARS-CoV-2 ORF10, a putative 38-amino acid viral protein encoded in the 3′ accessory region of the genome, is a highly ordered, hydrophobic, and thermally stable protein, which contains at least one transmembrane region [34,35]. The ORF10 binds to components of a Cullin-2-RING-ligase (CRL2) complex containing Cullin-2, RBX1, Elongin B, Elongin C, and ZYG11B ($CRL2^{ZY\ G11B}$) [36–38]. Earlier, it has been reported that the extreme N terminus of ORF10 contains a methionine-glycine-tyrosine motif, which would presumably aid ORF10 to be recruited into the $CRL2^{ZY\ G11B}$ ubiquitin ligase complex [37]. It was further confirmed that interaction between ORF10 and $CRL2^{ZY\ G11B}$ is not relevant for SARS-CoV-2 infection *in vitro* [37,39]. There is no evidence of ORF10 regulating or being regulated by $CRL2^{ZY\ G11B}$ [37]. On the other hand, the ORF10 protein in some SARS-CoV-2 variants, resulted in non-attenuation of disease and maintained transmissibility [40]. Furthermore, ORF10 is not essential for viral infection and replication while encoding a truncated protein that is neutrally evolving, through positive selection [39,41].

In this study, we report 128 single mutations and 35 co-occurring mutations in the unique SARS-CoV-2 ORF10 variants. This report illuminates potential effects due to mutations and co-occurring mutations in the emerging ORF10 variants from the secondary structure and intrinsic protein disorder perspectives.

2. Materials and methods

2.1. Data

A total of 202,968 SARS-CoV-2 ORF10 amino acid sequences were retrieved from the National Center for Biotechnology Information (NCBI) database on June 29, 2021. Note that none of these ORF10 sequences contained any ambiguous characters. Among the 202,968 SARS-CoV-2 ORF10 sequences only 140 were unique and contained amino acid substitutions that made them different from the ORF10 sequence found in the original hCoV-19/Wuhan/WIV04/2019 strain. Furthermore, SARS-CoV-2 ORF10 protein sequences from the GISAID database were used for finding the co-occurring mutations in the CoVal database.

2.2. Methods

2.2.1. Transmembrane topology and secondary structure prediction

Prediction of a transmembrane protein topology of a given protein is one of the classical issues in bioinformatics. The Phobius program was used to predict transmembrane topology for SARS-CoV-2 ORF10 protein variants [42,43].

The secondary structure of the SARS-CoV-2 ORF10 protein was predicted using the JPred 4 webserver [44]. In addition to protein secondary structure JPred was used to predict solvent accessibility and coiled-coil regions. The following keys were used in the secondary structure prediction of ORF10 variants [44].

- Shades of red: The more red a position is, the higher the level of conservation of chemical properties of the amino acids.
- Jnetpred: Final secondary structure prediction for a query.
- Jnet 25: Jnet prediction of burial, less than 25% solvent accessibility.
- Jnet 5: Jnet prediction of burial, less than 5% exposure.
- Jnet 0: Jnet prediction of burial, 0% exposure.
- Jnetconf: Jnet reliability of prediction accuracy ranges from 0 to 9, bigger is better.

2.2.2. Intrinsic disorder analysis

All SARS-CoV-2 ORF10 variants were subjected to the per-residue disorder analysis, with PONDR-VSL2 algorithm [45]. This tool showed good performance on proteins containing both structure and disorder, and is considered as an accurate standalone disorder predictor [46–48]. Predisposition scores for the per-residual conditions are 0 to 1, where 0 indicates residues entirely arranged, and 1 indicates residues completely disordered. Residues with predicted disorder scores between 0.25 and 0.5 were considered as moderately disordered, residues with disorder scores between 0.1 and 0.25 were considered flexible, whereas residues with the values of the predicted disorder scores higher than 0.5 were considered disordered.

2.2.3. Analysis of sequence variation

Single mutations in all the 140 unique ORF10 proteins were determined using the Virus Pathogen Resource ViPR by uploading a Fasta file of ORF10 sequences [49]. A snapshot of the ORF10 sequence variations is presented in Fig. 1.

Furthermore, the predicted effect on pathogenicity of all the mutations was analyzed with PredictSNP and PhD-SNP [50,51]. Note that PredictSNP web server makes a consensus based on other prediction tools such as MAPP, PolyPhen-1 and PolyPhen-2, SIFT, SNAP, and

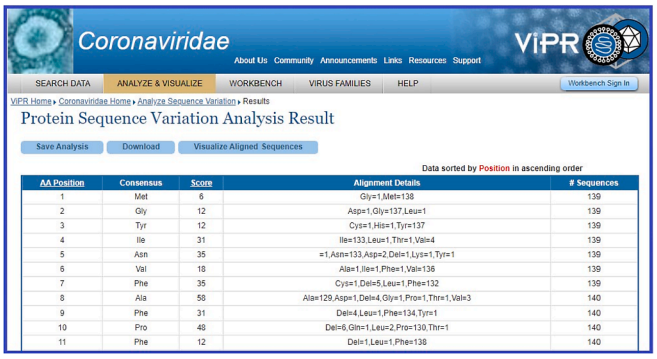

Fig. 1. A snapshot of ViPR database showing the ORF10 sequence variations and consensus amino acid residues.

PANTHER. Therefore, the degree of accuracy is expected to be high. The pathogenicity score (PredictSNP consensus prediction) was calculated using the following equation:

$$Pathogenicity\ Score = \left(\frac{\sum_{i=1}^{N}(\delta_i S_i)}{\sum_{i=1}^{N} S_i}\right) \times 100$$

where N is the number of integrated tools, δ_i represents the overall prediction (+1 for the deleterious prediction, -1 for the neutral prediction) and S_i expresses the transformed confidence scores [52].

In addition, co-occurring of mutations in ORF10 proteins were also detected by the CoVal database.

A quantitative measure was defined to localize the co-occurring mutations in the ORF10 protein in a given geo-location with regards to other geo-locations worldwide.

Localization across countries: For each co-occurring mutation in the ORF10 protein, localization is defined as

$$NF_m = \frac{NG_m}{TG_m}$$

where, NG_m and TG_m denote the number of SARS-CoV-2 genomes with these specific simultaneous mutations (m) in a geo-location, and the total number of SARS-CoV-2 genomes with this mutation (m) worldwide, respectively. It varies from 0 to 1. The normalized factor 0 denotes uniformly spreading of the mutations across various geo-locations, whereas 1 denotes the detection of the mutation in a single geo-location (discussed in CoVal database).

2.2.4. Frequency distribution of amino acids and clustering

The frequency distribution of each amino acid present in the ORF10 sequence was determined using standard bioinformatics routine in Matlab [53]. For each ORF10 sequence, a twenty-dimensional frequency-vector considering the frequency of standard twenty amino acids can be obtained. The distance (Euclidean metric) between any two pairs of frequency vectors was calculated for each pair of ORF10 sequences. By having the distance matrix, a set of clusters was obtained applying the well-known *K-means* clustering method using the standard routine in *Matlab-2021a* [53,54].

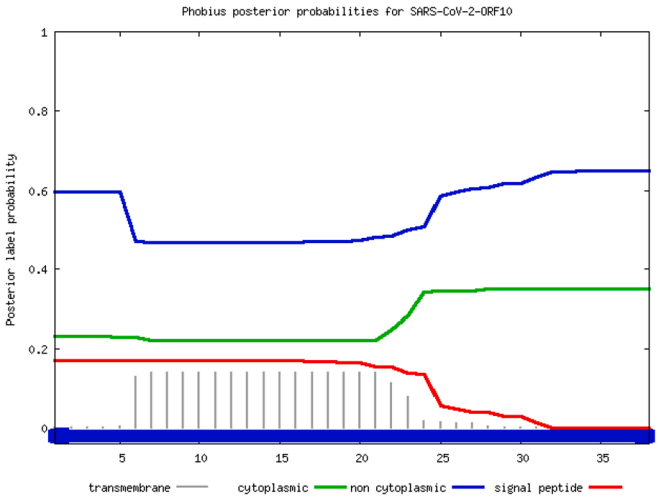

Fig. 2. Posterior probability plot for prediction of transmembrane topology and signal peptides for the wild-type SARS-CoV-2 ORF10.

Table 2
Continent-wise amino acid positions of single-mutations in SARS-CoV-2 ORF10 unique variants.

Continent-wise residue positions of single-mutations					
Africa	Asia	Europe	North America	Oceania	South America
3	6	3	1–38 (except 18th)	3	3
5	7	6		4	19
7	8	13		8	23
10	9	23		10	28
23	10	30		17	35
24	13	31		22	
28	14			23	
30	22			24	
31	23			28	
33	24			30	
37	30			37	
38	31			38	
	33				
	35				
	37				

3. Results

3.1. Continent-wise unique ORF10 variants and mutations

Continent-wise unique variations of ORF10 proteins and their mutations with predicted effects are presented in the following subsections.

3.1.1. ORF10 variants and transmembrane topology of SARS-CoV-2 ORF10

Continent-wise distribution of the total 140 unique ORF10 variants is presented in Table 1. The highest frequency of unique ORF10 variants was found in North America among the total of 140 SARS-CoV-2 ORF10 variants.

Continent-wise, a decreasing order percentage of unique ORF10 variants was Africa>South America>Europe>Asia>Oceania>North

Table 1
Unique mutations in the unique ORF10 variants across six continents. # denotes "number".

	Africa	Asia	Europe	North America	Oceania	South America
# of total ORF10	1183	3393	1033	186,572	10,290	497
# of unique ORF10	15	21	7	132	15	6
% of unique ORF10	1.27	0.62	0.68	0.07	0.15	1.21
# of residue positions of mutations in ORF10	12	15	6	37	12	5
% of total number of residues	31.6	39.5	15.8	97.4	31.6	13.2

Table 3
The predicted effect of ORF10 single mutations on pathogenicity.

Predicted effect of mutations							
Percentage of pathogenicity				Percentage of pathogenicity			
Mutation	PredictSNP	PhD-SNP	Predicted type	Mutation	PredictSNP	PhD-SNP	Predicted type
V33A	83%	66%	Neutral	N22H	83%	51%	Neutral
V33D	87%	77%	Deleterious	N22I	87%	61%	Deleterious
V33F	83%	45%	Neutral	N22K	87%	77%	Deleterious
V33I	83%	78%	Neutral	N22S	83%	68%	Neutral
D31G	87%	73%	Deleterious	N22T	87%	61%	Deleterious
D31H	87%	58%	Deleterious	N22Y	87%	73%	Deleterious
D31N	87%	68%	Deleterious	I4L	83%	78%	Neutral
D31V	87%	82%	Deleterious	I4T	83%	55%	Neutral
D31Y	87%	86%	Deleterious	I4V	83%	83%	Neutral
T38A	83%	78%	Neutral	R20G	87%	58%	Deleterious
T38I	83%	55%	Neutral	R20I	83%	68%	Neutral
L37F	83%	83%	Neutral	R20K	83%	68%	Neutral
L37H	83%	58%	Neutral	R20T	83%	51%	Neutral
L37I	83%	83%	Neutral	M21I	83%	51%	Neutral
L37P	87%	61%	Deleterious	M21K	87%	82%	Deleterious
L37R	87%	61%	Deleterious	M21L	87%	58%	Deleterious
Y3C	83%	58%	Neutral	M21T	87%	73%	Deleterious
Y3H	83%	72%	Neutral	M21V	83%	58%	Neutral
N5D	83%	66%	Neutral	N25D	83%	45%	Neutral
N5K	83%	55%	Neutral	N25G	87%	59%	Deleterious
N5S	83%	66%	Neutral	N25S	83%	55%	Neutral
N5Y	87%	68%	Deleterious	Y26C	87%	68%	Deleterious
R24C	87%	61%	Deleterious	Y26F	83%	68%	Neutral
R24H	83%	51%	Neutral	Y26H	83%	58%	Neutral
R24L	87%	61%	Deleterious	I27K	87%	86%	Deleterious
R24S	83%	58%	Neutral	I27L	83%	51%	Neutral
S23F	87%	58%	Deleterious	I27M	87%	58%	Deleterious
S23P	83%	51%	Neutral	I27R	87%	86%	Deleterious
P10L	87%	86%	Deleterious	I27T	87%	77%	Deleterious
P10Q	7%	73%	Deleterious	I27V	83%	66%	Neutral
P10S	83%	51%	Neutral	D31G	87%	73%	Deleterious
P10T	87%	68%	Deleterious	D31H	87%	58%	Deleterious
F7C	87%	59%	Deleterious	D31N	87%	68%	Deleterious
F7L	83%	55%	Neutral	D31V	87%	82%	Deleterious
F7S	83%	55%	Neutral	D31Y	87%	86%	Deleterious
V6A	83%	78%	Neutral	M1G	83%	72%	Neutral
V6F	83%	55%	Neutral	G2D	83%	68%	Neutral
V6I	83%	78%	Neutral	G2L	83%	58%	Neutral
Y14C	87%	68%	Deleterious	F11L	87%	73%	Deleterious
Y14F	83%	72%	Neutral	F11S	87%	61%	Deleterious
Y14H	83%	55%	Neutral	T12A	83%	58%	Neutral
A28P	87%	73%	Deleterious	T12M	87%	73%	Deleterious
A28S	83%	51%	Neutral	S15C	83%	51%	Neutral
A28V	83%	55%	Neutral	S15G	83%	58%	Neutral
V30A	83%	55%	Neutral	L16P	87%	86%	Deleterious
V30I	83%	78%	Neutral	L17F	83%	72%	Neutral
V30L	83%	51%	Neutral	L17P	87%	86%	Deleterious
F35C	87%	59%	Deleterious	C19F	87%	59%	Deleterious
F35S	83%	51%	Neutral	S23F	87%	58%	Deleterious
A8D	87%	77%	Deleterious	S23P	83%	51%	Neutral
A8G	83%	68%	Neutral	Q29H	83%	55%	Neutral
A8P	87%	73%	Deleterious	Q29L	87%	61%	Deleterious
A8S	83%	55%	Neutral	Q29R	87%	58%	Deleterious
A8V	83%	58%	Neutral	V32A	83%	66%	Neutral
F9L	87%	61%	Deleterious	V32I	83%	78%	Neutral
F9S	87%	58%	Deleterious	V32L	83%	55%	Neutral
F9Y	83%	51%	Neutral	N34D	83%	66%	Neutral
I13L	83%	55%	Neutral	N34Y	87%	73%	Deleterious
I13M	83%	51%	Neutral	N36K	83%	51%	Neutral
I13T	87%	61%	Deleterious	N36S	83%	72%	Neutral
I13V	83%	68%	Neutral	T38A	83%	78%	Neutral
N22D	83%	58%	Neutral	T38I	83%	55%	Neutral
N22F	83%	55%	Neutral				

America (Table 1).

In addition, the transmembrane topology and signal peptides for the wild-type SARS-CoV-2 ORF10 (YP 009725255) protein were predicted using the Phobius webserver. The associated posterior probability for the topology prediction is presented in Fig. 2.

From the posterior probability distributions, it was observed that the SARS-CoV-2 ORF10 protein was entirely non-cytoplasmic (Fig. 2).

3.1.2. *Unique ORF10 variants and their single and co-occurring mutations*

The amino acid residue positions of SARS-CoV-2 ORF10 single-mutations on each continent are listed in Table 2.

It was noticed that except for the residue in position 18, all amino

Table 4
Co-occurring mutations in the ORF10 variants in various geo-locations.

Mutations	Frequency	Date first collected	Localization across countries
USA			
M1K; G2A; Y3D; I4G; N5L; V6Y; F7K; A8R	9	16-01-2021	0.75
P10S; L37F	9	30-11-2020	1
P10L; R24C	2	17-03-2021	1
R24L; A28V	2	01-04-2021	1
C19F; A28V	1	24-03-2021	1
I4V; N5D	1	07-04-2021	1
L37F; T38I	1	09-12-2020	0.5
M1G; G2L	1	18-03-2020	0.4
M1Q; Y3R; I4W; N5A; V6I; A8T	1	23-02-2021	0.5
M1R; G2W; Y3A	1	30-03-2021	0.5
M1R; G2W; Y3A; N5T; V6F	1	22-07-2020	1
M21I; R24C	1	06-04-2021	1
N36C; T38I	1	08-03-2021	1
S23F; I27K	1	02-01-2021	1
UK			
M1G; G2L	2	01-05-2020	0.4
Q29I; V30F; D31N; V32C; N34T; F35L; N36G; L37R	1	29-04-2020	1
R20I; A28V	1	21-05-2020	1
T12M; V30L	1	18-01-2021	0.5
India			
A8L; F9I	1	09-03-2021	1
M1Q; Y3R; I4W; N5A; V6I; A8T	1	11-02-2021	0.5
P10S; F11V	1	23-04-2021	1
South Africa			
R24C; V30L	1	06-01-2021	0.4
Spain			
V30L; T38I	20	20-01-2021	0.95
P10S; V30L	13	20-01-2021	0.39
V30L; D31N	8	12-02-2021	0.8
V30L; L37F	4	18-01-2021	0.54
M1L; G2R; Y3P; I4K; N5L; V6M; F7Q	3	11-03-2020	1
R24C; V30L	2	01-03-2021	0.4
S23F; V30L	1	20-01-2021	0.38
Germany			
P10S; V30L	15	24-02-2021	0.39
V30L; D31H	4	11-03-2021	1
L16P; V30L	3	16-03-2021	1
P10S; S23F	3	28-03-2021	1
F7V; A8T	1	10-04-2021	1
L17I; R20I; V30L	1	2021-01	1
L37F; T38I	1	06-04-2021	0.5
S23F; V30L	1	2020-12	0.38
T12M; V30L	1	24-03-2021	0.5
Greece			
I13M; V30L	1	26-02-2021	1
Mexico			
M1K; G2A; Y3D; I4G; N5L; V6Y; F7K; A8R	1	09-04-2021	0.75
P10S; F35S	1	21-03-2021	1
Russia			
R20T; M21R; S23P; R24A; Y26N; I27A; Q29I; D31L; V32Q; V33L; N34P; F35Q; N36G; L37T	1	21-03-2020	1

acids at each position from 1 to 38 possessed point-missense mutations (Table 2). The common residue was S23, where two mutations S23F and S23P were found across all six continents. A total of eight common residue positions with mutations were observed in Asia and Africa, whereas several common residual mutation positions were associated with Asia and Oceania.

The predicted effects of pathogenicity for each mutation are listed in Table 3. Our data revealed that among a total of 128 mutations, 72 were neutral, and 56 deleterious with regards to pathogenicity.

Among a total of 37 residue positions with single mutations, the residue positions 1, 2, 11, 12, 15, 16, 20, 21, 25, 26, 27, 29, 32, 34, and 36 were unique in North America. Among all these residue positions, only the mutations at positions 11 and 16 in ORF10 variants in North America were predicted to be deleterious.

Furthermore, co-occurring mutations in the SARS-CoV-2 ORF10 in some geo-locations were listed in Table 4. The highest number of simultaneous mutations (at 14 positions among the total of 38 amino acid residues) in ORF10 was noticed in a SARS-CoV-2 variant from Russia on March 21, 2020. Interestingly, no report of this kind of co-occurring mutation globally, hence denoted by localized index 1.

Several co-occurring mutations in SARS-CoV-2 ORF10 variants have been reported in the USA, UK, India, South Africa, Spain, Germany, Greece, Mexico, and Russia. The most co-occurring mutations (V30L, T38I, first reported on January 20, 2021) were found in 20 infected patients in Spain. In the US the first detected and reported co-occurring mutations were M1K, G2A, Y3D, I4G, N5L, V6Y, F7K, and A8R on January 16, 2021 from 9 infected patients, and later on April 9 the first case was reported in Germany (Table 4). It is worth knowing that no single mutation at the residue positions 1 and 2 have been reported, and none of the co-occurring mutations among M1K, G2A, Y3D, I4G, N5L, V6Y, F7K, and A8R were reported as a single mutation in the ORF10 variants. Double co-occurring mutations P10S; V30l were reported in Spain on January 20, 2021, and on February 24, 2021, in Germany. Surprisingly, the pathogenic effects were predicted to be neutral (Table 3). It was noticed that V30L, one of the most common mutations in ORF10, was co-occurring with most of the other co-occurring mutations. Furthermore it was noticed that many mutations such as L17I, A8T, V6M, N34P, and F35Q did not appear as a single mutation, they appeared as one of the co-occurring mutations. It appears that co-occurring mutations in the SARS-CoV-2 ORF10 variants is an emerging trend.

3.2. Intrinsic disorder regions of SARS-CoV-2 ORF10 variants

The per-residue disorder profiles for 138 unique SARS-CoV-2 ORF10 variants (variants are too short for disorder analysis) and 35 co-occurring mutations are presented in Fig. 3. Fig. 3A shows that the intrinsic disorder predisposition of ORF10 is noticeably affected by single mutations. Mutations present the largest effects at the N- and C-terminal regions, where the disorder predisposition can vary from 0.4 to 0.8 and from 0.55 to 0.9 for the N- and C-termini, respectively, and for a region centered at residue 25, where the disorder score can change from 0.059 to 0.27. Fig. 3B compares the outputs of PONDR-VSL2 for 138 unique ORF10 variants with the results generated by one of the most conservative predictors of intrinsic disorder, and IUPred short [55].

Here, we investigate the effects of point mutations on the overall disorder score for the entire protein. This analysis showed that although the disorder score values generated by IUPred short are noticeably smaller than the corresponding PONDR-VSL2 data, the scales of changes introduced by single mutations in intrinsic disorder predisposition of ORF10 as evaluated by IUPred (from 0.03 to 0.095) are comparable to that generated by PONDR VSL2 (from 0.15 to 0.23). Furthermore, both predictors mostly agree on the direction of the changes introduced in the global disorder propensity of this protein by single mutations. Fig. 3C shows how disorder propensity is changed in ORF10 variants with co-occurring mutations. Noticeably, the effects of co-occurring mutants are qualitatively similar to those of single mutations, as most variability is observed at the disorder predisposition of N- and C-terminal regions and a region centered at residue 25. However, in the case of co-occurring mutants, scales of changes at the terminal regions are noticeably larger (the disorder predisposition can vary from 0.35 to 0.92 and from 0.2 to 0.9 for the N- and C-termini, respectively). Finally, to simplify comparison of the effect of co-occurring mutations on the disorder predisposition of ORF10, Fig. 3D shows “difference spectra” calculated by

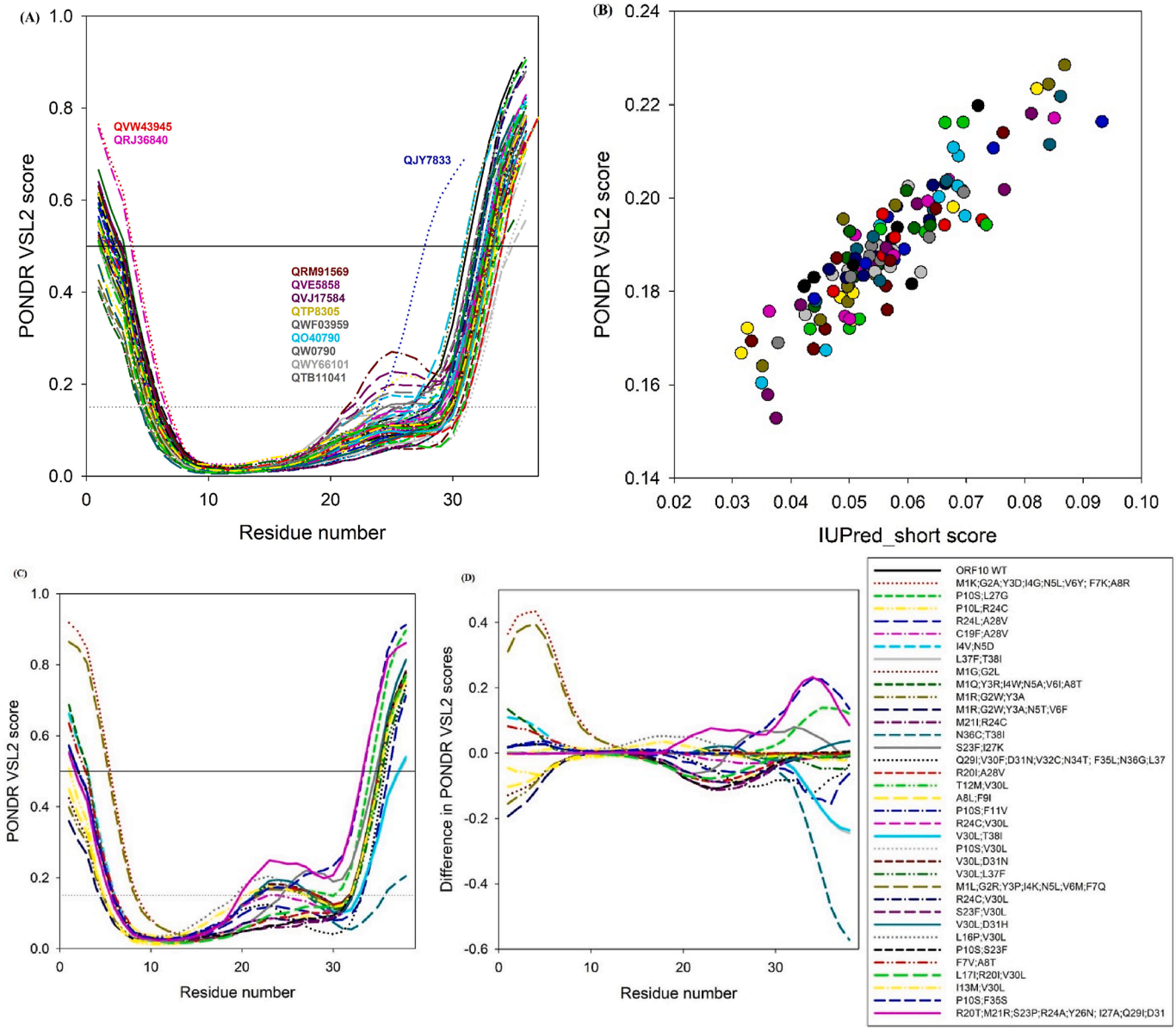

Fig. 3. (A): Per-residue disorder profiles for 138 SARS-CoV-2 ORF10 variants, (B): correlation between the outputs of two commonly used disorder predictors, (C): disorder propensity is changed in ORF10 variants with co-occurring mutations, and (D): difference spectra calculated by subtracting of the per-residue disorder scores of wild type ORF10 from the per-residue disorder scores of corresponding mutants.

subtracting of the per-residue disorder scores of wild type ORF10 from the per-residue disorder scores of corresponding mutants. In this plot, intensities of the resulting "bands" reflect the magnitude of changes, whereas their sign, reflects the mutation-induced increase or decrease (positive or negative values, respectively) in local disorder propensity. Fig. 3D shows that most of the co-occurring mutations increase the disorder predisposition of the N-terminal region of ORF10, whereas many such mutations decrease the disorder propensity of the region centered at residue 25, and most of the mutations do not affect disorder predisposition of the C-terminal region.

Since ORF10 is not an enzyme, the accumulating point and co-occurring mutations are likely to affect some other functions of this protein, e.g., its capability to be engaged in protein-protein interactions. In fact, as discussed in the following section, accumulated data suggested the presence of multiple host partner proteins for ORF10. In fact, Fig. 3 shows that ORF10 is a short hybrid protein containing disordered tails and a more ordered central region; it is likely that this protein is using both ordered and disordered segments for its interactions.

3.3. Interactability of ORF10 and intrinsic disorder status of its host partners

The SARS-CoV-2 ORF10 protein was found to interact with few of the human proteins such as CUL2, ELOB, ELOC, MAP7D1, PPT1, RBX1, THTPA, TIMM8B, and ZYG11B [37]. A detailed summary of the tissue and cellular expression patterns of SARS-CoV-2 ORF10 interacting human proteins, based on transcriptomics and antibody-based proteomics, are presented in Fig. 5. The ORF10 of SARS-CoV-2 interacts with members of the Cullin ubiquitin ligase $CUL2^{ZY\ G11B}$ complex. Interestingly, among the genes, ZYG11B scored the highest with regards to ORF10 interactome, which confirmed a direct interaction between ORF10 and ZYG11B [36].

The SARS-CoV-2 ORF10 interacting with human proteins CUL2, ELOB, PPT1, THTPA, and TIMM8B were ex- pressed in various tissues,

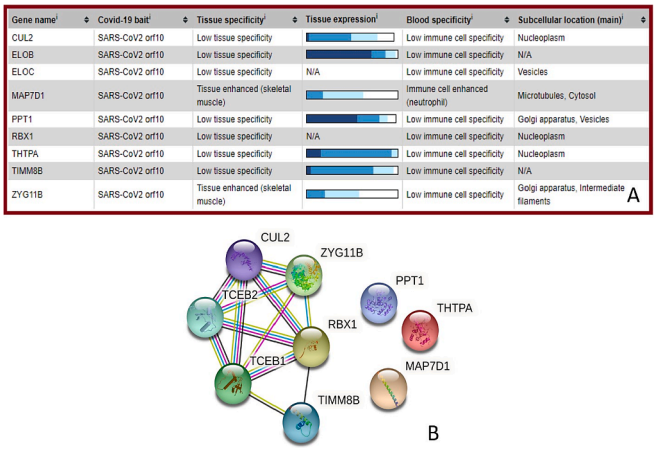

Gene name	Covid-19 bait	Tissue specificity	Tissue expression	Blood specificity	Subcellular location (main)
CUL2	SARS-CoV2 orf10	Low tissue specificity		Low immune cell specificity	Nucleoplasm
ELOB	SARS-CoV2 orf10	Low tissue specificity		Low immune cell specificity	N/A
ELOC	SARS-CoV2 orf10	Low tissue specificity	N/A	Low immune cell specificity	Vesicles
MAP7D1	SARS-CoV2 orf10	Tissue enhanced (skeletal muscle)		Immune cell enhanced (neutrophil)	Microtubules, Cytosol
PPT1	SARS-CoV2 orf10	Low tissue specificity		Low immune cell specificity	Golgi apparatus, Vesicles
RBX1	SARS-CoV2 orf10	Low tissue specificity	N/A	Low immune cell specificity	Nucleoplasm
THTPA	SARS-CoV2 orf10	Low tissue specificity		Low immune cell specificity	Nucleoplasm
TIMM8B	SARS-CoV2 orf10	Low tissue specificity		Low immune cell specificity	N/A
ZYG11B	SARS-CoV2 orf10	Tissue enhanced (skeletal muscle)		Low immune cell specificity	Golgi apparatus, Intermediate filaments

A

Fig. 4. A: A snapshot summary of the tissue and cellular expression patterns of SARS-CoV-2 ORF10 interacting human proteins, based on transcriptomics and antibody-based proteomics. B: Inter-set protein-protein interaction network of human proteins interacting with ORF10 generated by Search Tool for the Retrieval of Interacting Genes; STRING, http://string-db.org/. STRING produces a network of protein- protein interactions based on predicted and experimentally-validated information on the interaction partners of a protein of interest [56]. In the corresponding network, the nodes correspond to proteins, whereas the edges show predicted or known functional associations. Seven types of evidence are used to build the corresponding network, where they are indicated by the differently colored lines: a green line represents neighborhood evidence; a red line – the presence of fusion evidence; a purple line – experimental evidence; a blue line – co-occurring evidence; a light blue line – database evidence; a yellow line – text mining evidence; and a black line – co-expression evidence [56]. (For interpretation of the references to color in this figure legend, the reader is referred to the web version of this article.)

including the lung. SARS-CoV-2 ORF10 contains an α-helical region (amino acid residue positions 3 to 20), which may interact and form a complex with $CUL2^{ZY\ G11B}$ [36]. It was furthermore reported that by forming a complex with $CUL2^{ZY\ G11B}$, ORF10 hijacks it for ubiquitination and degradation of restriction factors, or alternatively, may bind to the N-terminal glycine in ORF10 to target it for degradation [36,37].

Fig. 4B represents the STRING-generated network of the host proteins interacting with ORF10 and demonstrates that CUL2, ZYG11B, RBX1, ELOB/TCEB1, ELOC/TCEB2, and TIMM8B form a tightly linked cluster, whereas PPT1, THTPA, and MAP7D1 are not involved in interaction with other host proteins considered here [56]. Intrinsic disorder profiles for these proteins, ranging from 83 (TIMM88) to 841 residues (MAD7D1), are presented in Fig. 5. These profiles generated a set of commonly used disorder predictors and show that ORF10 interacting proteins possess rather different levels of intrinsic disorder, with some of them being mostly ordered (e.g., PPT1, which is an expected feature of an enzyme), and others (e.g., MAP7D1) being highly disordered. In fact, based on their increasing disorder content evaluated by PONDR-VSL2 as a percent of predicted intrinsically disordered residues (PPIDR), these proteins can be arranged into the following sequence: PPT1 (3.59%) < ZYG11B (9.41%) < THTPA (22.17%) < CUL2 (22.5%) < ELOC/TCEB2 (23.21%) < RBX1 (29.63%) < TIMM8B (44.58%) < ELOB/TCEB1 (74.58%) < MAD7D1 (98.93%).

Therefore, based on the accepted classification, proteins are considered as mostly ordered, moderately disordered and highly disordered if their PPDR < 10%, $10 \leq PPDR < 30\%$, and highly disordered PPDR ≥ 30%, respectively, PPT1 and ZYG11B are highly ordered, THTPA, CUL2, and ELOC/TCEB2 are moderately disordered, and RBX1, TIMM8B, ELOB/TCEB1, and MAD7D1 are highly disordered [61].

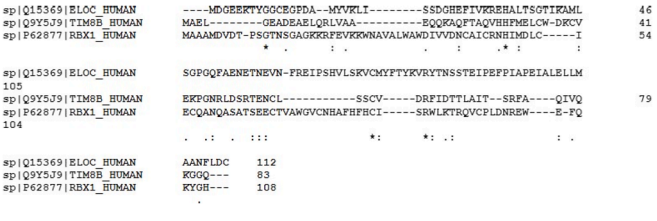

```
sp|Q15369|ELOC_HUMAN      ----MDGEERTYGGCEGPDA--MYVKLI--------SSDGHEFIVKREHALTSGTIKAML      46
sp|Q9Y5J9|TIM8B_HUMAN     MAEL--------GEADEAELQRLVAA----------EQQKAQFTAQVHHFMELCW-DKCV      41
sp|P62877|RBX1_HUMAN      MAAAMDVDT-PSGTNSGAGKKRFEVKKWNAVALWAWDIVVDNCAICRNHIMDLC-----I      54
                                 *  .     : .          .    :    .* :       :

sp|Q15369|ELOC_HUMAN      SGPGQFAENETNEVN-FREIPSHVLSKVCMYFTYKVRYTNSSTEIPEFPIAPEIALELLM
105
sp|Q9Y5J9|TIM8B_HUMAN     EKPGNRLDSRTENCL----------SSCV-----DRFIDTTLAIT--SRFA----QIVQ      79
sp|P62877|RBX1_HUMAN      ECQANQASATSEECTVAWGVCNHAFHFHCI-----SRWLKTRQVCPLDNREW----E-FQ
104
                                 . .:  .  :::              *:     *: .:             : .

sp|Q15369|ELOC_HUMAN      AANFLDC    112
sp|Q9Y5J9|TIM8B_HUMAN     KGGQ---    83
sp|P62877|RBX1_HUMAN      KYGH---    108
                                 .
```

Fig. 5. Intrinsic disorder predisposition of human proteins interacting with ORF10 (A: CUL2; B: ZYG11B; C: PPT1; D: THTPA; E: ELOB; F: ELOC; G: TIMM8B; H: RBX1; and I: MAD7D1) analyzed by six per-residue predictors, PONDR-VLXT, PONDR-VSL2, PONDR-VL3, PONDR-FIT, and the IUPred2A computational platform that allows identification of either short or long regions of intrinsic disorder, IUPred-L and IUPred-S [56–60]. The outputs of the evaluation of the per-residue disorder propensity by these tools are represented as real numbers between 1 (ideal prediction of disorder) and 0 (ideal prediction of order). A threshold of ≥0.5 was used to identify disordered residues and regions in query proteins. For each query protein in this study, the predicted percentage of intrinsic disorder (PPID) was calculated based on the outputs of per-residue disorder predictors. Here, PPID in a query protein represents a percent of residues with disorder scores exceeding 0.5.

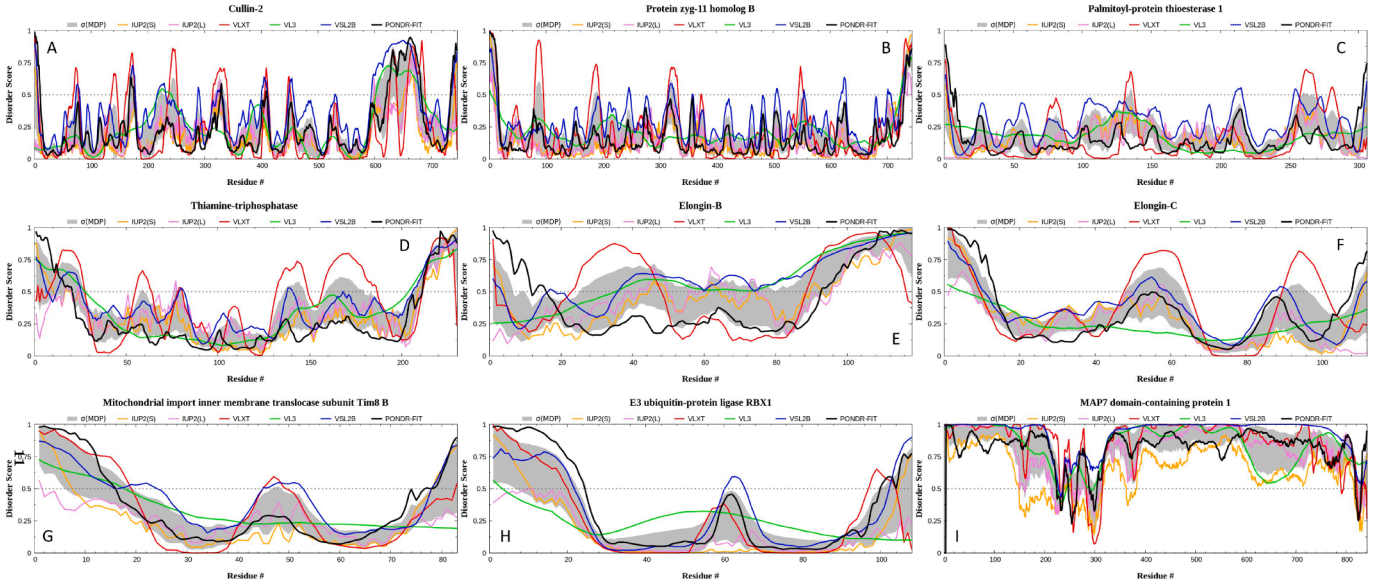

Fig. 6. Sequence alignment among ELOC, TIM8B, and RBX1 human proteins.

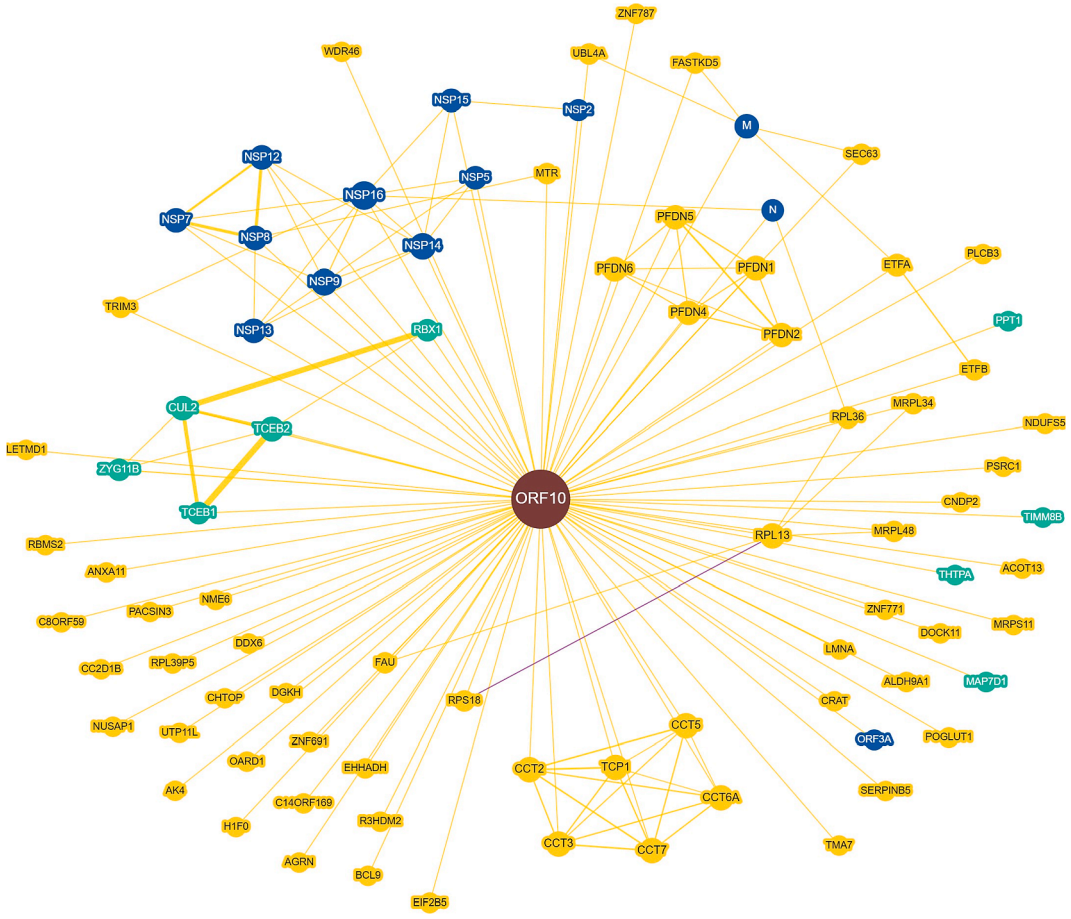

Fig. 7. ORF10-centered protein-protein interaction network generated by BioGRID. This network includes both human and SARS-CoV-2 proteins engaged in interaction with ORF10 (dark red circle in the middle of the plot). Nine human proteins discussed in the previous section are shown in green, whereas the remaining human proteins are shown by yellow symbols. Blue symbols correspond to proteins from SARS-CoV-2. Yellow lines represent interactions with physical evidence, purple lines show association with genetic and physical evidence. Node size reflects the number of edges to/from that node, with the larger node possessing more edges attached to it. Similarly, the edge thickness serves as a reflection of the number of unique curated interactions supporting the association, with thicker lines representing edges with more unique curated interactions supporting its existence. (For interpretation of the references to color in this figure legend, the reader is referred to the web version of this article.)

Curiously, Fig. 5 shows close similarity of the disorder profiles of TIMM88 and RBX1, and to a latter degree, ELOB/TCEB1 despite the fact that these three proteins are characterized by relatively low sequence identity (ranging from 11.69 to 25.64%) (Fig. 6):

We further looked at the presence of potential disorder-based binding sites (molecular recognition features, MoRFs; i.e., disordered regions that gain ordered structure at interaction with binding partners) in these nine proteins using the ANCHOR algorithm [62]. This analysis revealed that more than half of these proteins contains MoRFs: ZYG11B (residues 716-721), CUL2 (residues 679-688), ELOB (residues 1-6 and 75-96), THTPA (residues 1-6 and 193-200), and MAD7D1 (residues 1-22, 37-80, 88-107, 115-125, 132-142, 149-163, 232-237, 251-268, 291-315, 336-345, 355-386, 398-406, 408-414, 427-491, 500-550,565-608, 635-642, 713-719, 737-762, 772-799, and 814-832), suggesting the role of intrinsic disorder in their functionality. This analysis indicates that at least some of these MoRFs can be involved in interaction with ORF10. Obviously, subsequent experimental analysis is needed to verify this interesting hypothesis.

To further extend the interactability analysis of ORF10, we used a Biological General Repository for Interaction Datasets BioGRID platform, which is a comprehensively curated biomedical interaction repository containing 2,133,831 protein and genetic interactions, 29,417 chemical interactions, and 1,128,339 post translational modifications from major model organism species [63]. One of the recent BioGRID activities is a COVID-19 coronavirus curation project, where 15,645 non-redundant interactions are described for 32 SARS-CoV-2 proteins. Fig. 7 represents a protein-protein inter- action (PPI) network generated by BioGRID for ORF10. This network 72 contains 72 host proteins (including 9 proteins discussed in the previous sections) and 12 SARS-CoV-2 proteins. These data indicate that despite its small size, ORF10 is a highly promiscuous protein interacting with multiple host proteins and potentially affecting a multitude of functional pathways in the host. It is also likely that the unique mutations found in the natural variants of this protein can affect its interactability and associated multi-functionality, generating highly heterogeneous outputs (Fig. 8).

Analysis of this network in terms of the significantly enriched Gene Ontology terms (GO-terms) indicated that the molecular functions of its proteins include unfolded protein binding, structural constituent of ribosome, and RNA binding. Furthermore, the 37 significantly enriched GO-terms corresponding to biological processes include positive regulation of establishment of protein localization to telomere (GO:1904851), positive regulation of protein localization to Cajal body (GO:1904871), positive regulation of telomerase RNA localization to Cajal body (GO:1904874), positive regulation of telomere maintenance via telomerase (GO:0032212), binding of sperm to zona pellucida (GO:0007339), toxin transport (GO:1901998), regulation of telomere maintenance (GO:0032204), fatty acid beta-oxidation (GO:0006635), regulation of protein localization to nucleus (GO:1900180), SRP-

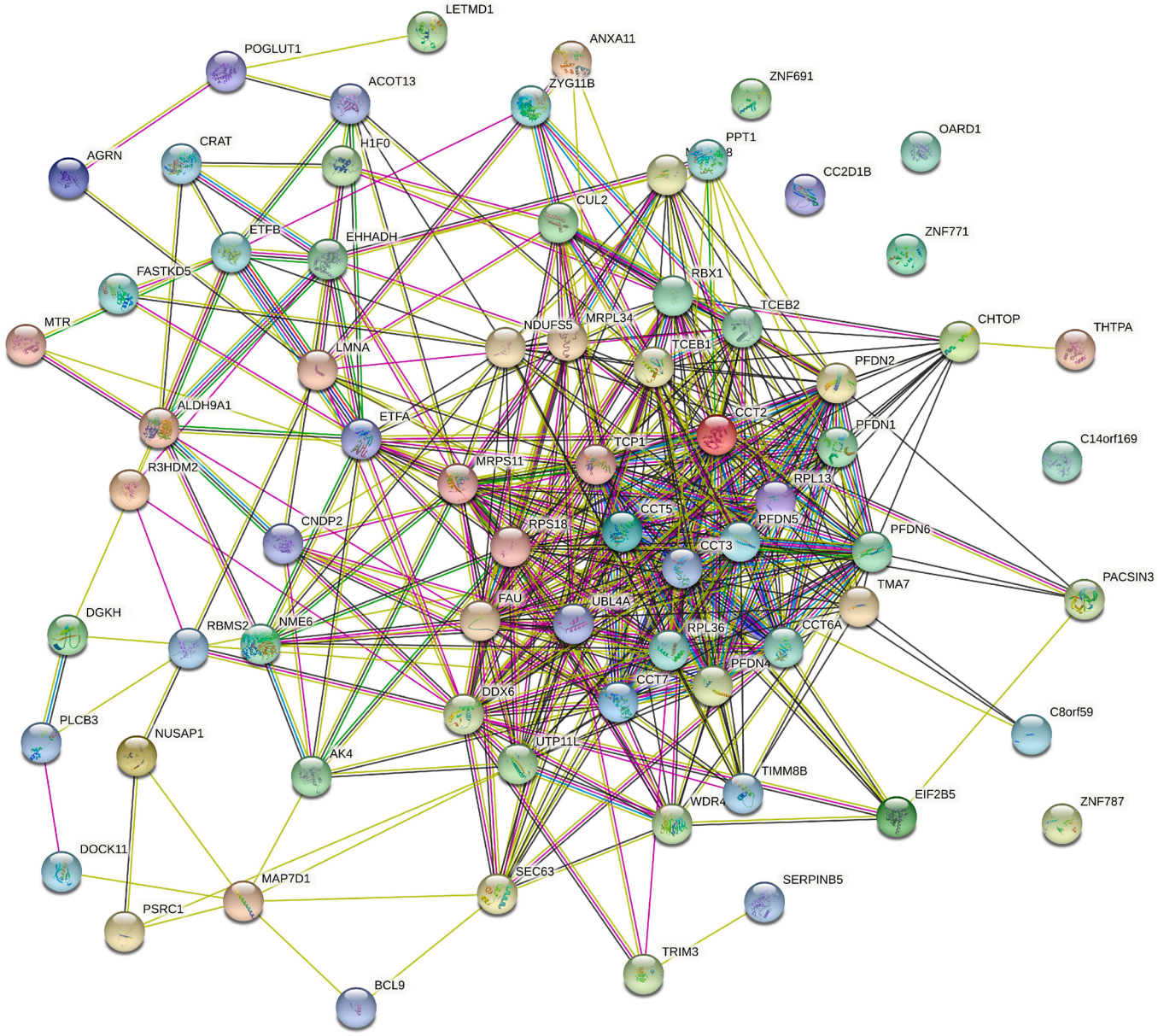

Fig. 8. STRING-based analysis of the inter-set interactivity of 72 human proteins interacting with SARS-CoV-2 ORF10 using the low confidence level of 0.15. This confidence level was selected to ensure maximal inclusion of host proteins into the resulting PPI.

dependent cotranslational protein targeting to membrane (GO:0006614), protein folding (GO:0006457), regulation of transcription from RNA polymerase II promoter in response to hypoxia (GO:0061418), positive regulation of chromosome organization (GO:2001252), translational initiation (GO:0006413), protein stabilization (GO:0050821), cellular response to hypoxia (GO:0071456), peptide biosynthetic process (GO:0043043), regulation of chromosome organization (GO:0033044), translation (GO:0006412), regulation of protein stability (GO:0031647), protein targeting (GO:0006605), regulation of DNA metabolic process (GO:0051052), amide biosynthetic process (GO:0043604), establishment of protein localization to organelle (GO:0072594), positive regulation of organelle organization (GO:0010638), cellular amide metabolic process (GO:0043603), protein localization to organelle (GO:0033365), cellular macromolecule catabolic process (GO:0044265), organonitrogen compound biosynthetic process (GO:1901566), positive regulation of cellular component organization (GO:0051130), macromolecule catabolic process (GO:0009057), cellular nitrogen compound biosynthetic process (GO:0044271), organic substance catabolic process (GO:1901575), cellular catabolic process (GO:0044248), cellular nitrogen compound metabolic process (GO:0034641), cellular metabolic process (GO:0044237), and cellular process (GO:0009987). It is tempting therefore to hypothesize that at least part of these functions and processes will be affected by ORF10 via its binding to specific host proteins.

One should keep in mind that each of these human proteins interacting with ORF10 is a promiscuous binder itself. This is illustrated by Table 5 that provides some basic information about these host proteins. It is seen that with almost no exception, these proteins are engaged in multiple interactions, often serving as hubs of corresponding PPI networks. As high binding promiscuity is often associated with the presence of intrinsic disorder in a query of proteins, we also analyzed intrinsic disorder predispositions of these host proteins. Corresponding data are shown in Table 5 and Fig. 9. Based on the accepted practice, per-protein features derived from the corresponding disorder profiles can be used to classify proteins as mostly ordered, moderately or highly disordered. This analysis revealed that only four proteins are expected to be mostly

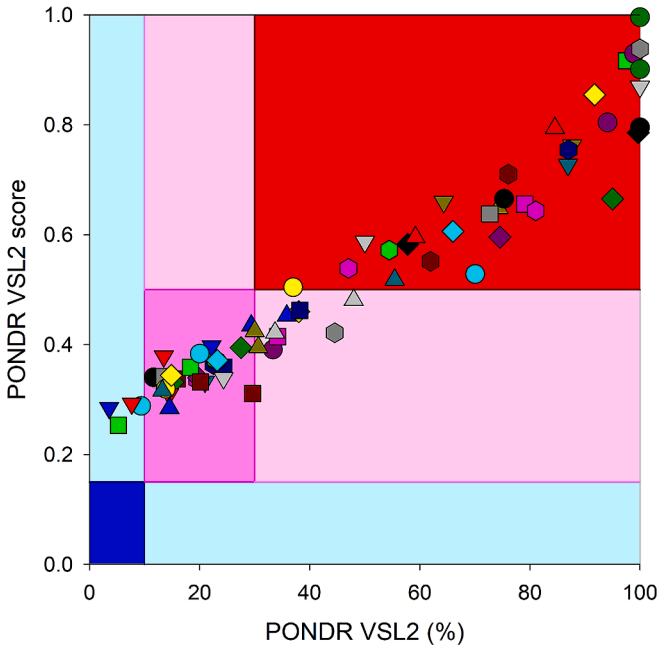

Fig. 9. Intrinsic disorder predisposition of 72 human proteins interacting with SARS-CoV-2 ORF10 protein based on their mean disorder scores and percent of predicted disordered residues as evaluated by PONDR(R) VSL2 algorithm. Large values of each parameter indicate increasing disorder. Color blocks indicate regions which are mostly ordered (blue and light blue), moderately disordered (pink and light pink), or mostly disordered (red). If the two parameters agree, the corresponding part of the background is dark (blue or pink), whereas light blue and light pink reflect areas in which only one of these criteria applies. It is noteworthy that only four human proteins that interact with ORF10 are mostly (located within the light blue area). The remaining 68 proteins are either moderately or highly disordered. (For interpretation of the references to color in this figure legend, the reader is referred to the web version of this article.)

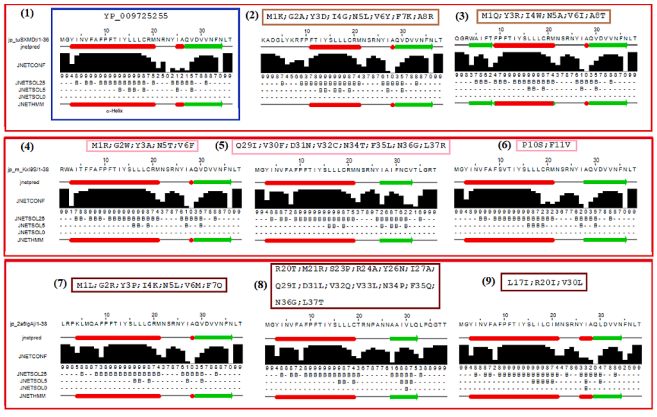

Fig. 10. Secondary structure predispositions of nine ORF10 variants including the wild ORF10 (YP 009725255) with co-occurring mutations as predicted by the JPred 4 webserver [44]. Red and green stretches correspond to the predicted α-helices and β-strands, respectively. (For interpretation of the references to color in this figure legend, the reader is referred to the web version of this article.)

ordered, 43 are highly disordered and 25 are moderately disordered. Furthermore, most of the 72 human proteins contain MoRFs (see Table 5), and all of these proteins can undergo extensive post translational modifications (PTMs, data not shown). This is not surprising, as many enzymatically-catalyzed PTMs are commonly found within the intrinsically disordered or flexible regions [64–66]. These observations indicate that these host proteins utilize their intrinsic disorder for

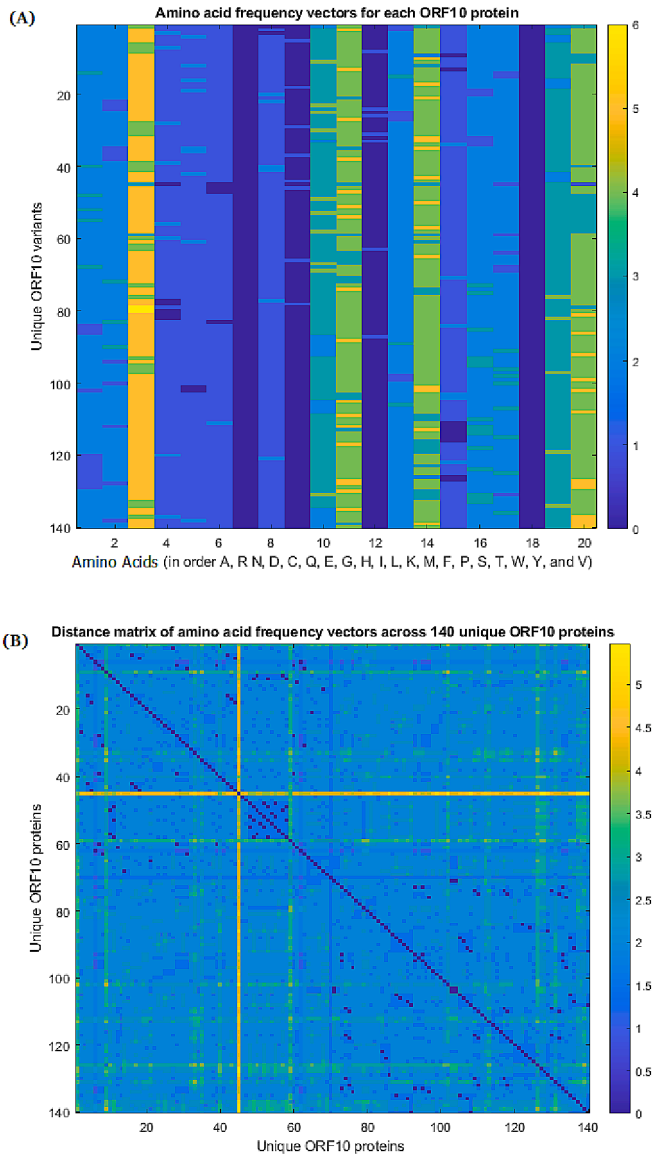

Fig. 11. (A): Frequency distribution of amino acids across the unique 140 ORF10 proteins, and (B) pairwise distance matrix of frequency vectors for each ORF10 protein

interaction with specific partners (including ORF10) and for modulation of these interactions via PTMs.

3.4. Predicting secondary structures of ORF10 protein variants with co-occurring mutations

The secondary structures of nine ORF10 variants including the wild-type ORF10 (YP 009725255) with several co-occurring mutations were predicted (Fig. 10). The α-helix secondary structural amino acid (aa) residue positions 3 to 20 were invariant for the six ORF variants with co-occurring mutations as mentioned in panels (4) to (9) of Fig. 10, although the reliability indices were changed for the α-helix region [36].

Furthermore, it was observed that the α-helix amino acid residue positions (3-20) were switched to 11-21 and 9-21 due to the co-occurring mutations M1K, G2A, Y3D, I4G, N5L, V6Y, F7K, A8R, and M1Q, Y3R, I4W, N5A, V6I, A8T in two different ORF10 variants, respectively. Therefore, due to these two sets of co-occurring mutations, SARS-CoV-2 ORF10 interactions with the $CUL2^{ZY\ G11B}$ complex might be affected. Due to the amino acid residue positional changes in the secondary structure in the ORF10 variants (other than the reference ORF10

Table 5
Interactability and intrinsic disorder of human proteins interacting with ORF10. Proteins are arranged by their intrinsic disorder content and lines are colored in red, pink and blue to show highly disordered, moderately disordered and highly ordered proteins, respectively.

Gene	Protein	UniProt ID	Length	NSTRING (confidence)	NBioGRID	PPIDR (%)	MoRFs
CHTOP	Chromatin target of PRMT1 protein	Q9Y3Y2	248	140 (0.4)	127	100.0	7
FAU	40S ribosomal protein S30	P62861	59	98 (0.4)	99	100.0	1 (whole protein)
PSRC1	Proline/serine-rich coiled-coil protein 1	Q6PGN9	363	78 (0.4)	31	100.0	8
RPL39P5	Putative 60S ribosomal protein L39-like 5	Q59GN2	51	Not found	Not found	100.0	1 (whole protein)
TMA7	Translation machinery-associated protein 7	Q9Y2S6	64	73 (0.4)	27	100.0	2
ZNF771	Zinc finger protein 771	Q7L3S4	317	13 (0.4)	21	99.7	3
MAP7D1	**MAP7 domain-containing protein 1**	**Q3KQU3**	**841**	**33 (0.4)**	**79**	**98.9**	**22**
BCL9	B-cell CLL/lymphoma 9 protein	O00512	1,426	125 (0.4)	20	97.5	23
C8orf59	Ribosomal biogenesis facto	Q8NoT1	100	13 (0.4)	6	95.0	4
NUSAP1	Nucleolar and spindle-associated protein 1	Q9BXS6	441	210 (0.4)	52	94.1	13
H1F0	Histone H1.0	P07305	194	223 (0.4)	126	91.7	7
LMNA	Prelamin-A/C	P02545	664	404 (0.4)	915	87.7	12
ZNF691	Zinc finger protein 691	Q5VV52	315	12 (0.4)	16	87.0	5
ZNF787	Zinc finger protein 787	Q6DD87	382	42 (0.4)	20	86.9	2
R3HDM2	R3H domain-containing protein 2	Q9Y2K5	976	47 (0.4)	119	84.5	23
RPL13	60S ribosomal protein L13	P26373	211	436 (0.4)	335	81.1	5
RPL36	60S ribosomal protein L36	Q9Y3U8	105	374 (0.4)	215	79.1	3
CC2D1B	Coiled-coil and C2 domain-containing protein 1B	Q5T0F9	858	78 (0.4)	30	76.1	11
PFDN2	Prefoldin subunit 2	Q9UHV9	154	196 (0.4)	128	75.3	2
TCEB2	**Elongin-B**	**Q15370**	**118**	**287 (0.4)**	**243**	**74.6**	**2**
UTP11L	Probable U3 small nucleolar RNA-associated protein 11	Q9Y3A2	253	313 (0.4)	24	74.3	4
RBMS2	RNA-binding motif, single-stranded-interacting protein 2	Q15434	407	53 (0.4)	59	72.7	11
UBL4A	Ubiquitin-like protein 4A	P11441	157	255 (0.4)	338	70.1	0
PACSIN3	Protein kinase C and casein kinase substrate in neurons protein 3	Q9UKS6	424	59 (0.4)	102	66.0	6
PFDN6	Prefoldin subunit 6	O15212	129	186 (0.4)	85	64.3	1
PFDN4	Prefoldin subunit 4	Q9NQP4	134	90 (0.4)	91	61.9	1
ANXA11	Annexin A11	P50995	505	54 (0.4)	67	59.2	4
AGRN	Agrin	O00468	2,068	202 (0.4)	231	57.8	3
MRPL34	39S ribosomal protein L34, mitochondrial	Q9BQ48	92	125 (0.4)	42	55.4	2
PLCB3	1-Phosphatidylinositol 4,5-bisphosphate phosphodiesterase beta-3	Q01970	1,234	202 (0.4)	29	54.5	15
PFDN1	Prefoldin subunit 1	O60925	122	124 (0.4)	117	50.0	0
TRIM3	Tripartite motif-containing protein 3	O75382	744	45 (0.4)	59	48.0	6
WDR46	WD repeat-containing protein 46	O15213	610	315 (0.4)	124	47.1	7
TIMM8B	**Mitochondrial import inner membrane translocase subunit Tim8 B**	**Q9Y5J9**	**83**	**86 (0.4)**	**40**	**44.6**	**0**
C14orf169	Ribosomal oxygenase 1	Q9H6W3	641	59 (0.4)	29	38.2	3
SEC63	Translocation protein SEC63 homolog	Q9UGP8	760	101 (0.4)	101	38.0	10
PFDN5	Prefoldin subunit 5	Q99471	154	301 (0.4)	203	37.0	0
NDUFS5	NADH dehydrogenase [ubiquinone] iron-sulfur protein 5	O43920	106	210 (0.4)	138	35.9	0
RPS18	40S ribosomal protein S18	P62269	152	417 (0.5)	268	34.2	1
EIF2B5	Translation initiation factor eIF-2B subunit epsilon	Q13144	721	87 (0.4)	78	33.7	5
SERPINB5	Serpin B5	P36952	375	119 (0.4)	111	33.3	0
MRPL48	39S ribosomal protein L48, mitochondrial	Q96GC5	212	132 (0.4)	111	30.7	0
DGKH	Diacylglycerol kinase eta	Q86XP1	1,220	84 (0.4)	24	30.0	2
RBX1	**E3 ubiquitin-protein ligase RBX1**	**P62877**	**108**	**456 (0.5)**	**431**	**29.6**	**0**
MRPS11	28S ribosomal protein S11, mitochondrial	P82912	194	354 (0.4)	174	29.4	3
DDX6	Probable ATP-dependent RNA helicase DDX6	P26196	485	293 (0.4)	248	27.5	3
DOCK11	Dedicator of cytokinesis protein 11	Q5JSL3	2,073	50 (0.4)	22	24.4	3
OARD1	ADP-ribose glycohydrolase OARD1	Q9Y530	152	48 (0.4)	17	24.3	0
TCEB1	**Elongin-C**	**Q15369**	**112**	**273 (0.4)**	**196**	**23.2**	**0**
EHHADH	Peroxisomal bifunctional enzyme	Q08426	723	199 (0.4)	144	23.1	0
CCT5	T-complex protein 1 subunit epsilon	P48643	541	488 (0.4)	347	22.9	2
CUL2	**Cullin-2**	**Q13617**	**742**	**196 (0.4)**	**507**	**22.6**	**0**
THTPA	**Thiamine-triphosphatase**	**Q9BU02**	**230**	**38 (0.4)**	**21**	**22.2**	**2**
NME6	Nucleoside diphosphate kinase 6	O75414	186	110 (0.4)	17	21.0	0
FASTKD5	FAST kinase domain-containing protein 5, mitochondrial	Q7L8L6	764	56 (0.4)	250	20.2	2
ETFB	Electron transfer flavoprotein subunit beta	P38117	255	164 (0.4)	125	20.0	0
CRAT	Carnitine O-acetyltransferase	P43155	626	106 (0.4)	17	19.8	0
ETFA	Electron transfer flavoprotein subunit alpha, mitochondrial	P13804	333	206 (0.4)	208	19.5	0
CCT3	T-complex protein 1 subunit gamma	P49368	545	431 (0.4)	425	18.3	3
CCT2	T-complex protein 1 subunit beta	P78371	353	452 (0.45)	455	15.9	0
CNDP2	Cytosolic non-specific dipeptidase	Q96KP4	475	135 (0.4)	60	15.2	1
CCT6A	T-complex protein 1 subunit zeta	P40227	531	389 (0.4)	385	14.9	0
MTR	Methionine synthase	Q99707	1,265	117 (0.4)	54	14.5	1
POGLUT1	Protein O-glucosyltransferase 1	Q8NBL1	392	52 (0.4)	41	14.5	0
TCP1	T-complex protein 1 subunit alpha	P17987	556	447 (0.4)	370	13.8	0
ACOT13	Acyl-coenzyme A thioesterase 13	Q9NPJ3	140	95 (0.4)	37	13.6	0
CCT7	T-complex protein 1 subunit eta	Q99832	543	458 (0.4)	385	13.3	1
AK4	Adenylate kinase 4, mitochondrial	P27144	223	98 (0.4)	99	11.7	0
ZYG11B	**Protein zyg-11 homolog B**	**Q9C0D3**	**744**	**53 (0.4)**	**56**	**9.4**	**1**
ALDH9A1	4-Trimethylaminobutyraldehyde dehydrogenase	P49189	494	108 (0.4)	41	7.7	0
LETMD1	LETM1 domain-containing protein 1	Q6P1Q0	360	22 (0.4)	54	5.3	0

(YP 009725255)), these ORF10 variants with human proteins other than the $CUL2^{ZY\ G11B}$ complex are likely to be affected. Mutations at position 1 affect the methionine initiation codon, for which replacement only valine has been shown to support translation of protein. As for the ORF10 mutations methionine at position 1 is replaced by arginine (M1R), glutamine (M1Q), leucine (M1L), and lysine (M1K), respectively, the mutants should not code for protein and therefore possess no secondary structure.

3.5. Amino acid frequency distribution across the unique ORF10 variants and associated clusters

The frequency of each amino acid in the 140 unique ORF10 sequences is presented in Tables 6 and 7. Also, Fig. 11(A) shows the amino acid frequency vector of each unique ORF10 sequence. It was noticed that glutamic acid (E) and tryptophan (W) were absent in each ORF10 variant. Among 140 unique ORF10 variants, lysine (K) was present with a single frequency only in seven North American ORF10 variants (QTD22916.1, QLA48060.1, QWY66101.1, QVO40425.1, QTP28305.1, QSL79091.1, and QRM91569.1).

Table 6
Frequency distribution of amino acids over the 140 unique SARS-CoV-2 ORF10 variants (from QKM75696.1 to QWN58574.1).

ORF10	A	R	N	D	C	Q	E	G	H	I	L	K	M	F	P	S	T	W	Y	V
QKM75696.1	2	2	4	1	1	1	0	0	0	2	4	0	1	3	1	2	2	0	2	3
QKG88643.1	2	2	5	1	1	1	0	1	0	3	5	0	1	4	1	2	2	0	3	4
QVJ13930.1	2	2	5	2	1	1	0	0	0	3	4	0	2	4	1	2	2	0	3	4
QWE67724.1	2	2	5	1	2	1	0	1	0	3	4	0	2	4	1	2	2	0	2	4
QRJ36840.1	2	2	5	1	1	1	0	1	1	3	4	0	2	4	1	2	2	0	2	4
QQY03084.1	2	2	4	1	1	1	0	1	0	3	4	0	2	4	1	2	2	0	3	4
QRG22086.1	2	2	4	2	1	1	0	1	0	3	4	0	2	4	1	2	2	0	3	4
QTD22916.1	2	2	4	1	1	1	0	1	0	3	4	1	2	4	1	2	2	0	3	4
QUL69971.1	2	2	5	1	1	1	0	1	0	3	4	0	2	2	0	2	2	0	3	3
QWB85197.1	2	2	5	1	1	1	0	1	0	3	4	0	2	5	1	2	2	0	3	3
QWJ83116.1	2	2	5	1	1	1	0	1	0	4	4	0	2	4	1	2	2	0	3	3
QSE09446.1	2	2	5	1	2	1	0	1	0	3	4	0	2	3	1	2	2	0	3	4
QWZ00470.1	2	2	5	1	1	1	0	1	0	3	5	0	2	4	0	2	2	0	3	4
QTP26076.1	3	2	5	1	1	1	0	1	0	3	4	0	2	4	1	2	1	0	3	4
QWK62875.1	2	2	5	1	1	1	0	1	0	3	4	0	3	4	1	2	1	0	3	4
QVG57396.1	2	2	5	1	2	1	0	1	0	3	4	0	2	4	1	2	2	0	2	4
QRA60944.1	2	2	5	1	1	1	0	1	0	3	4	0	2	5	1	2	2	0	2	4
QWE68295.1	2	2	5	1	1	1	0	1	1	3	4	0	2	4	1	2	2	0	2	4
QWT58729.1	2	2	5	1	2	1	0	1	0	3	4	0	2	4	1	1	2	0	3	4
QWM42669.1	2	2	5	1	1	1	0	2	0	3	4	0	2	4	1	1	2	0	3	4
QWS64226.1	2	2	5	1	1	1	0	1	0	3	3	0	2	5	1	2	2	0	3	4
QVJ47956.1	2	1	5	1	1	1	0	2	0	3	4	0	2	4	1	2	2	0	3	4
QVW78101.1	2	1	5	1	1	1	0	1	0	4	4	0	2	4	1	2	2	0	3	4
QLA48060.1	2	1	5	1	1	1	0	1	0	3	4	1	2	4	1	2	2	0	3	4
QVO98764.1	2	2	5	1	1	1	0	1	0	4	4	0	1	4	1	2	2	0	3	4
QWY66101.1	2	2	5	1	1	1	0	1	0	3	4	1	1	4	1	2	2	0	3	4
QWQ05246.1	2	2	5	1	1	1	0	1	0	3	5	0	1	4	1	2	2	0	3	4
QTS35265.1	2	2	4	2	1	1	0	1	0	3	4	0	2	4	1	2	2	0	3	4
QVP24786.1	2	2	4	1	1	1	0	1	1	3	4	0	2	4	1	2	2	0	3	4
QVO85840.1	2	2	4	1	1	1	0	1	0	4	4	0	2	4	1	2	2	0	3	4
QVO40425.1	2	2	4	1	1	1	0	1	0	3	4	1	2	4	1	2	2	0	3	4
QWU52456.1	2	2	5	1	1	1	0	1	0	3	4	0	2	5	1	1	2	0	3	4
QTP28305.1	2	2	5	1	1	1	0	1	0	2	4	1	2	5	1	1	2	0	3	4
QWS07290.1	2	2	5	1	1	1	0	1	0	3	4	0	2	4	2	1	2	0	3	4
QWF07009.1	2	1	5	1	2	1	0	1	0	3	3	0	2	5	1	2	2	0	3	4
QWY19801.1	2	1	5	1	2	1	0	1	0	3	4	0	2	4	1	2	2	0	3	4
QWX30181.1	2	1	5	1	1	1	0	1	1	3	4	0	2	4	1	2	2	0	3	4
QWY95666.1	2	1	5	1	1	1	0	1	0	3	5	0	2	4	1	2	2	0	3	4
QVU00656.1	2	2	4	2	1	1	0	1	0	3	4	0	2	4	1	2	2	0	3	4
QTA53643.1	3	2	4	1	1	1	0	2	0	3	4	0	2	4	1	2	2	0	3	3
QUG14309.1	2	2	4	1	1	1	0	2	0	3	4	0	2	4	1	2	2	0	3	4
QWY70751.1	2	2	5	1	2	1	0	1	0	3	4	0	2	4	1	2	2	0	2	4
QSJ35636.1	2	2	5	1	1	1	0	1	0	3	4	0	2	5	1	2	2	0	2	4
QWF03959.1	2	2	5	1	1	1	0	1	1	3	4	0	2	4	1	2	2	0	2	4
BCY15724.1	2	2	3	0	1	0	0	1	0	3	3	0	2	3	1	2	1	0	3	1
QWT72678.1	2	2	5	1	1	0	0	1	1	3	4	0	2	4	1	2	2	0	3	4
QUM42028.1	2	2	5	1	1	0	0	1	0	3	5	0	2	4	1	2	2	0	3	4
QUX49292.1	3	2	5	1	1	1	0	1	0	3	4	0	2	4	1	2	2	0	3	3
QWK69365.1	2	2	5	1	1	1	0	1	0	4	4	0	2	4	1	2	2	0	3	3
QTA74333.1	2	2	5	1	1	1	0	1	0	3	4	0	2	5	1	2	2	0	3	3
QWY54619.1	2	2	5	1	1	1	0	1	0	3	5	0	2	4	1	2	2	0	3	3
QUV26065.1	3	2	5	1	1	1	0	1	0	3	4	0	2	4	1	2	2	0	3	3
QWF05003.1	2	2	5	1	1	1	0	1	0	4	4	0	2	4	1	2	2	0	3	3
QUP00476.1	2	2	5	1	1	1	0	1	0	3	5	0	2	4	1	2	2	0	3	3
QTJ93574.1	3	2	5	1	1	1	0	1	0	3	4	0	2	4	1	2	2	0	3	3
QWN49685.1	2	2	5	2	1	1	0	1	0	3	4	0	2	4	1	2	2	0	3	3
QVO91006.1	2	2	5	1	1	1	0	1	0	3	4	0	2	5	1	2	2	0	3	3
QVV18442.1	2	2	5	1	1	1	0	1	0	4	4	0	2	4	1	2	2	0	3	3
QJY78233.1	2	2	3	1	1	1	0	1	0	3	3	0	2	3	1	2	1	0	3	4
QVL90897.1	2	2	4	2	1	1	0	1	0	3	4	0	2	4	1	2	2	0	3	4
QOH29638.1	2	2	5	1	2	1	0	1	0	3	4	0	2	3	1	2	2	0	3	4
QWC74916.1	2	2	4	1	1	1	0	1	0	3	4	0	2	4	1	2	2	0	3	4
QSL79091.1	2	2	4	1	1	1	0	1	0	3	4	1	2	4	1	2	2	0	3	4
BCX23983.1	2	2	5	1	1	1	0	1	0	3	3	0	2	4	1	2	1	0	3	4
QWY94400.1	2	2	5	1	1	1	0	1	0	3	3	0	2	5	1	2	2	0	3	4
QSE25736.1	2	2	5	1	1	1	0	1	1	3	3	0	2	4	1	2	2	0	3	4
QWN58574.1	2	2	5	1	1	1	0	1	0	4	3	0	2	4	1	2	2	0	3	4

It was noticed that asparagine (N) was present in the ORF10 sequences with the highest frequencies ranging from 4 to 6 (Fig. 11(A)). Also, the frequencies of leucine (L), phenylalanine (F), and valine (V) in each ORF10 variant were dominant as compared to that of other amino acids.

For each pair of frequency vectors associated with ORF10 sequences, distances were enumerated (Fig. 11(B)).

The most distant frequency vector was detected for the SARS-CoV-2 ORF10 BCY15724.1 (Japan, collected in November, 2020). Based on frequency-vector similarity (Euclidean distance-wise nearness), unique

Table 7
Frequency distribution of amino acids over the 140 unique SARS-CoV-2 ORF10 variants (from QTI75440.1 to QWY55420.1).

ORF10	A	R	N	D	C	Q	E	G	H	I	L	K	M	F	P	S	T	W	Y	V
QTI75440.1	3	2	5	1	1	1	0	1	0	3	4	0	2	4	1	2	1	0	3	4
QWS53172.1	2	2	5	1	1	1	0	1	0	4	4	0	2	4	1	2	1	0	3	4
YP 009725255.1	2	2	5	1	1	1	0	1	0	3	4	0	2	4	1	2	2	0	3	4
QWY95092.1	2	2	5	1	1	1	0	1	0	3	3	0	2	4	2	2	2	0	3	4
QWQ66744.1	2	3	5	1	1	1	0	1	0	3	3	0	2	4	1	2	2	0	3	4
QSW62483.1	2	2	4	1	1	1	0	1	0	3	4	0	2	4	1	3	2	0	3	4
QVU28280.1	2	2	5	1	1	1	0	1	0	3	5	0	2	3	1	2	2	0	3	4
QWW53635.1	2	2	5	1	1	1	0	1	0	3	4	0	2	3	1	3	2	0	3	4
QQX05795.1	2	2	4	1	1	1	0	1	0	3	4	0	2	4	1	2	2	0	4	4
QVE28736.1	2	2	5	0	1	1	0	2	0	3	4	0	2	4	1	2	2	0	3	4
QTC84700.1	2	2	5	0	1	1	0	1	1	3	4	0	2	4	1	2	2	0	3	4
QWN49673.1	2	2	6	1	1	1	0	1	0	3	4	0	2	4	1	2	2	0	3	3
QUA36764.1	2	2	6	0	1	1	0	1	0	3	4	0	2	4	1	2	2	0	3	4
QSW42096.1	2	2	5	0	1	1	0	1	0	3	4	0	2	4	1	2	2	0	3	5
QWY22460.1	2	2	5	0	1	1	0	1	0	3	4	0	2	4	1	2	2	0	4	4
QUF19963.1	2	3	5	1	1	0	0	1	0	3	4	0	2	4	1	2	2	0	3	4
QTB11041.1	1	2	5	1	1	1	0	1	0	3	4	0	2	4	2	2	2	0	3	4
QWX09518.1	1	2	5	1	1	1	0	1	0	3	4	0	2	4	1	3	2	0	3	4
QWU01215.1	1	2	5	1	1	1	0	1	0	3	4	0	2	4	1	2	2	0	3	5
QRM91569.1	2	2	5	1	1	1	0	1	0	2	4	1	2	4	1	2	2	0	3	4
QRX03618.1	2	2	5	1	1	1	0	1	0	2	5	0	2	4	1	2	2	0	3	4
QSO40790.1	2	2	5	1	1	1	0	1	0	2	4	0	3	4	1	2	2	0	3	4
QVE25858.1	2	3	5	1	1	1	0	1	0	2	4	0	2	4	1	2	2	0	3	4
QVJ17584.1	2	2	5	1	1	1	0	1	0	2	4	0	2	4	1	2	3	0	3	4
QVO95200.1	2	2	5	1	1	1	0	1	0	2	4	0	2	4	1	2	2	0	3	5
QVE30392.1	2	2	4	1	1	1	0	1	0	3	4	0	2	4	1	3	2	0	3	4
QTC19517.1	2	1	5	1	1	1	0	1	0	3	4	0	2	4	1	3	2	0	3	4
QVJ37366.1	2	2	4	1	1	1	0	1	0	3	4	0	2	4	1	3	2	0	3	4
QWQ76823.1	2	2	4	1	1	1	0	1	0	3	4	0	2	4	1	2	3	0	3	4
QVV08801.1	2	2	4	1	1	1	0	1	0	3	4	0	2	4	1	2	2	0	4	4
QUI12106.1	2	2	5	1	1	1	0	1	0	3	4	0	1	4	1	2	3	0	3	4
QWU53472.1	2	2	5	1	1	1	0	1	0	3	4	0	1	4	1	2	2	0	3	5
QTS24551.1	2	1	5	1	1	1	0	1	0	3	4	0	2	4	1	2	3	0	3	4
QNV50343.1	2	2	5	1	0	1	0	1	0	3	4	0	2	5	1	2	2	0	3	4
QUB17908.1	1	2	5	1	0	1	0	1	0	3	4	0	2	5	1	2	2	0	3	5
QVL64016.1	2	2	5	1	1	1	0	1	0	3	3	0	2	4	2	2	2	0	3	4
QWU68360.1	2	2	5	1	1	1	0	1	0	3	3	0	2	4	2	2	2	0	3	4
QTO29824.1	2	2	5	1	1	1	0	1	0	2	5	0	2	4	1	2	2	0	3	4
QWU51246.1	2	2	5	1	1	1	0	1	0	2	4	0	3	4	1	2	2	0	3	4
QVX69392.1	2	2	5	1	1	1	0	1	0	2	4	0	2	4	1	2	3	0	3	4
QWO21857.1	2	2	5	1	1	1	0	1	0	2	4	0	2	4	1	2	2	0	3	5
QTK02152.1	2	2	5	1	1	1	0	1	0	3	5	0	2	3	1	2	2	0	3	4
QWY72735.1	2	2	5	1	1	1	0	1	0	3	4	0	2	3	1	3	2	0	3	4
QVH90751.1	2	2	5	1	1	2	0	1	0	3	4	0	2	4	0	2	2	0	3	4
QVX36355.1	2	1	5	1	1	1	0	1	0	3	5	0	2	4	0	3	2	0	3	4
QWY95104.1	2	2	5	1	1	1	0	1	0	3	3	0	2	5	0	3	2	0	3	4
QWY18545.1	2	2	5	1	1	1	0	1	0	3	4	0	2	4	0	3	2	0	3	4
QVL15727.1	2	2	5	1	1	1	0	1	0	3	4	0	2	4	0	2	3	0	3	4
QTO07027.1	2	2	5	1	1	1	0	1	0	3	4	0	2	3	0	2	2	0	3	4
BCX25240.1	2	2	5	1	1	1	0	1	0	3	5	0	2	3	1	2	2	0	3	4
QWB65585.1	2	2	5	1	1	1	0	1	0	3	4	0	2	3	1	3	2	0	3	4
QTW57386.1	2	2	5	1	1	1	0	1	0	3	4	0	2	3	1	2	2	0	4	4
QWW38212.1	1	2	5	2	1	1	0	1	0	3	4	0	2	4	1	2	2	0	3	4
QSE30156.1	1	2	5	1	1	1	0	2	0	3	4	0	2	4	1	2	2	0	3	4
QUF17645.1	1	2	5	1	1	1	0	1	0	3	4	0	2	4	2	2	2	0	3	4
QUF20717.1	1	2	5	1	1	1	0	1	0	3	4	0	2	3	1	2	2	0	3	4
QWB83606.1	1	2	5	1	1	1	0	1	0	3	4	0	2	4	1	3	2	0	3	4
QPF60767.1	1	2	5	1	1	1	0	1	0	3	4	0	2	4	1	2	3	0	3	4
QVR42407.1	1	2	5	1	1	1	0	1	0	3	4	0	2	2	0	2	2	0	3	4
QUA32182.1	1	2	5	1	1	1	0	1	0	3	5	0	2	4	0	2	2	0	3	5
QRG41735.1	1	1	5	1	1	1	0	1	0	3	5	0	2	4	1	2	2	0	3	5
QWT73590.1	1	2	5	1	1	1	0	1	0	3	4	0	2	4	1	2	2	0	3	5
QWK62266.1	2	2	5	1	1	1	0	1	0	3	5	0	2	3	1	2	2	0	3	4
QVM67662.1	2	2	5	1	1	1	0	1	0	4	4	0	2	3	1	3	1	0	3	4
QQE14148.1	2	2	5	1	1	1	0	1	0	3	4	0	2	3	1	3	2	0	3	4
QVU00728.1	2	2	4	1	1	1	0	1	0	3	4	0	2	4	1	3	2	0	3	4
QUA79573.1	2	2	4	1	1	1	0	1	0	3	4	0	2	4	1	2	2	0	4	4
QWT65692.1	2	2	5	1	1	1	0	1	0	2	5	0	2	4	1	2	2	0	3	4
QVW43945.1	2	2	5	1	1	1	0	1	0	2	4	0	2	4	1	2	3	0	3	4
QUM21266.1	2	2	4	2	1	1	0	1	0	2	4	0	2	4	1	2	2	0	3	5
QTX06599.1	2	1	5	1	2	1	0	1	0	2	4	0	2	4	1	2	2	0	3	5
QVM14069.1	2	2	5	1	1	1	0	1	0	2	3	0	2	5	1	2	2	0	3	5
QWY55420.1	2	2	5	1	1	1	0	1	0	2	4	0	2	4	1	2	2	0	3	5

Table 8
K-means clustering (clusters: 20) of the unique ORF10 variants based on amino acid frequency distribution.

ORF10	Cluster	ORF10	Cluster	ORF10	Cluster	ORF10	Cluster
QKM75696.1	8	QVW78101.1	11	BCY15724.1	17	QWN58574.1	15
QKG88643.1	1	QLA48060.1	1	QWT72678.1	16	QTI75440.1	16
QVJ13930.1	1	QVO98764.1	11	QUM42028.1	1	QWS53172.1	11
QWE67724.1	7	QWY66101.1	1	QUX49292.1	14	YP 009725255.1	5
QRJ36840.1	7	QWQ05246.1	1	QWK69365.1	11	QWY95092.1	15
QQY03084.1	5	QTS35265.1	20	QTA74333.1	3	QWQ66744.1	15
QRG22086.1	20	QVP24786.1	20	QWY54619.1	14	QSW62483.1	5
QTD22916.1	20	QVO85840.1	20	QUV26065.1	14	QVU28280.1	6
QUL69971.1	18	QVO40425.1	20	QWF05003.1	11	QWW53635.1	19
QWB85197.1	3	QWU52456.1	3	QUP00476.1	14	QQX05795.1	20
QWJ83116.1	11	QTP28305.1	10	QTJ93574.1	14	QVE28736.1	16
QSE09446.1	6	QWS07290.1	16	QWN49685.1	14	QTC84700.1	16
QWZ00470.1	1	QWF07009.1	10	QVO91006.1	3	QWN49673.1	14
QTP26076.1	16	QWY19801.1	1	QVV18442.1	11	QUA36764.1	16
QWK62875.1	16	QWX30181.1	1	QJY78233.1	8	QSW42096.1	4
QVG57396.1	7	QWY95666.1	1	QVL90897.1	20	QWY22460.1	16
QRA60944.1	3	QVU00656.1	20	QOH29638.1	6	QUF19963.1	16
QWE68295.1	7	QTA53643.1	16	QWC74916.1	5	QTB11041.1	4
QWT58729.1	16	QUG14309.1	20	QSL79091.1	20	QWX09518.1	4
QWM42669.1	16	QWY70751.1	7	BCX23983.1	15	QWU01215.1	4
QWS64226.1	3	QSJ35636.1	3	QWY94400.1	3	QRM91569.1	9
QVJ47956.1	1	QWF03959.1	7	QSE25736.1	15	QRX03618.1	12

ORF10	Cluster	ORF10	Cluster	ORF10	Cluster	ORF10	Cluster
QSO40790.1	9	QVH90751.1	1	QVU00728.1	5	QWU68360.1	15
QVE25858.1	9	QVX36355.1	2	QUA79573.1	20	QTO29824.1	12
QVJ17584.1	9	QWY95104.1	10	QWT65692.1	12	QWU51246.1	9
QVO95200.1	9	QWY18545.1	1	QVW43945.1	9	QVX69392.1	9
QVE30392.1	5	QVL15727.1	1	QUM21266.1	10	QWO21857.1	9
QTC19517.1	1	QTO07027.1	6	QTX06599.1	10	QTK02152.1	6
QVJ37366.1	5	BCX25240.1	6	QVM14069.1	10	QWY72735.1	19
QWQ76823.1	20	QWB65585.1	19	QWY55420.1	9		
QVV08801.1	20	QTW57386.1	6	QVR42407.1	18		
QUI12106.1	1	QWW38212.1	4	QUA32182.1	2		
QWU53472.1	4	QSE30156.1	4	QRG41735.1	2		
QTS24551.1	1	QUF17645.1	4	QWT73590.1	4		
QNV50343.1	3	QUF20717.1	6	QWK62266.1	6		
QUB17908.1	2	QWB83606.1	4	QVM67662.1	13		
QVL64016.1	15	QPF60767.1	4	QQE14148.1	19		

Table 9
Frequency of ORF10 variants in each cluster.

Cluster number	Frequency	Cluster number	Frequency	Cluster number	Frequency
1	17	5	7	19	4
20	14	11	7	12	3
16	13	14	7	8	2
4	11	15	7	18	2
9	10	7	6	13	1
3	9	10	6	17	1
6	9	2	4		

140 ORF10 proteins were clustered using the K-means clustering method (Table 8).

Based on amino acid compositions in each ORF10 sequence, unique ORF10 proteins were clustered into 20 different clusters. Cluster-1 contains the highest number (17) of ORF10 variants (which fall in the US), whereas clusters 13 and 17 contain only one ORF10 variant each. The ORF10 proteins BCY15724 (collected from Japan) and QVM67662 (USA: Florida) belong to cluster 13 and 17, respectively (Table 9).

Clearly, twenty different clusters with different frequencies of ORF10 variants showed wide variations of ORF10 sequences based on amino acid compositions.

4. Discussion

In this study, a total of 140 unique SARS-CoV-2 ORF10 sequences were observed among 202968 ORF10 sequences obtained from the NCBI database. Remarkably, most unique ORF10 variants were first reported in North America only (Table 1). Consequently, the highest number of point mutations and co-occurring mutations were found in North America. Continent-wise Africa had the highest percentage (1.27%) of unique variants of ORF10 sequences. Furthermore, it was observed that all amino acids of ORF10 except for residue 18, possessed single-missense mutations (Table 2). The unique ORF10 variants from Asia, Africa, and Oceania had several point-mutations at common residue positions (Table 2).

We noticed that in North America, ORF10 mutations only at the amino acid residue positions 11 (F11S, F11L) and 16 (L16P) were deleterious. A significant percentage of non-synonymous mutations, 53 among the total of 128 mutations were deleterious, which may alter the intensity of the interactome between ORF10 and host proteins. The 22 unique co-occurring mutations were observed in different geo-locations (Table 4). It was noticed that co-occurring mutations in ORF10 variants became an emerging trend, which varied slightly in 2020, and inevitably in future ORF10 variants with co-occurring mutations might be transmitted to other geo-locations while restriction on international travel are lifted. Furthermore, it was observed that the effects of co-occurring mutants are qualitatively similar to those of single mutations, as most variability is at the disorder predisposition of N- and C-terminal regions and a region centered at residue 25. However, in co-occurring mutants, scales of changes at the terminal regions are noticeably larger. Most of the co-occurring mutations increase the disorder predisposition of the N-terminal region of ORF10, whereas many such mutations decrease the

disorder propensity of the region centered at residue 25. Consequently, these mutations may affect the secondary structure and associated functions of the ORF10 variants. In addition, amino acid residue positions of the secondary structures (especially the N-terminal α-helix regions) of several ORF10 variants changed, and therefore interaction of those ORF10 variants with the human protein $CUL2^{ZY\ G11B}$ complex are most likely altered.

5. Conclusions

Unique variations in SARS-CoV-2 ORF10 proteins are an emerging trend across different continents due to the appearance of various single point and co-occurring mutations. The highest percentages of unique ORF10 variants were found in Africa, though the highest frequency of unique ORF10 variants was found in North America. Among the possible explanations for this phenomenon are: a) (world largest number of the sequenced SARS-CoV-2 isolates originates from North America); b) the existence of the co-infection between the different SARS-CoV-2 strains in North America (which is almost non-existent in the other parts of the world, with the noticeable exception for England) [67]; c) highly diversified population, which is traditionally separated into ethnically, racially, and culturally different enclaves; d) implementation of very different approaches for controlling the COVID-19 spread by local administrations potentially generating conditions for the locally diversified evolution of SARS-CoV-2.

It was further observed that the growth rate of emerging non-synonymous mutations in ORF10 proteins is increasing non-linearly, which is certainly alarming with regards to stability or instability of emerging SARS-CoV-2 variants. Due to significant deleterious mutations, expression of the SARS-CoV-2 ORF10 proteins might get altered, a phenomenon, which will affect functional virus-host protein-protein interactions. Also, it was reported that the secondary structure α helix regions of the ORF10 variants was changed due to co-occurring mutations. Consequently, virulence/pathogenicity of SARS-CoV-2 may get influenced directly or indirectly and therefore, continuous surveillance of mutations and their associated effects is necessary.

CRediT authorship contribution statement

Sk. Sarif Hassan: Conceptualization; Formal analysis; Investigation; Methodology; Research design; Supervision; Validation; Visualization; Writing – original draft; Writing – review & editing

Kenneth Lundstrom: Data curation; Formal analysis; Investigation; Writing – original draft; Writing – review & editing

Angel Serrano-Aroca: Data curation; Formal analysis; Investigation; Writing – review & editing

Parise Adadi: Data curation; Formal analysis; Investigation; Writing – review & editing

Alaa A. A. Aljabali: Data curation; Formal analysis; Investigation; Writing – review & editing

Elrashdy M. Redwan: Data curation; Formal analysis; Investigation; Writing – review & editing

Amos Lal: Data curation; Formal analysis; Investigation; Writing – review & editing

Ramesh Kandimalla: Data curation; Formal analysis; Investigation; Writing – review & editing

Tarek Mohamed Abd El-Aziz: Data curation; Formal analysis; Investigation; Writing – review & editing

Pabitra Pal Choudhury: Data curation; Formal analysis; Investigation; Writing – review & editing

Gajendra Kumar Azad: Data curation; Formal analysis; Investigation; Writing – review & editing

Samendra P Sherchan: Data curation; Formal analysis; Investigation; Writing – review & editing

Gaurav Chauhan: Data curation; Formal analysis; Investigation; Writing – review & editing

Murtaza Tambuwala: Data curation; Formal analysis; Investigation; Writing – review & editing

Kazuo Takayama: Data curation; Formal analysis; Investigation; Writing – review & editing

Debmalya Barh: Data curation; Formal analysis; Investigation; Writing – review & editing

Giorgio Palu: Data curation; Formal analysis; Investigation; Writing – review & editing

Pallab Basu: Data curation; Formal analysis; Investigation; Writing – review & editing

Vladimir N. Uversky: Conceptualization; Formal analysis; Investigation; Methodology; Research design; Supervision; Validation; Visualization; Writing – original draft; Writing – review & editing

All authors read the final article and approved it for submission.

Acknowledgements

We gratefully acknowledge the authors from the originating laboratories responsible for obtaining the specimens and the Submitting laboratories where genetic sequence data were generated and shared via the NCBI and GISAID Initiatives, on which this research is based.

References

[1] Worldometer, COVID live update. https://www.worldometers.info/coronavirus/. (Accessed 6 August 2021).
[2] Johns-Hopkin-University, Coronavirus Resource Center. https://coronavirus.jhu.edu/map.html. (Accessed 6 August 2021).
[3] S. Laha, J. Chakraborty, S. Das, S.K. Manna, S. Biswas, R. Chatterjee, Characterizations of SARS-CoV-2 mutational profile, spike protein stability and viral transmission, Infect. Genet. Evol. 85 (2020), 104445.
[4] J.-S. Kim, J.-H. Jang, J.-M. Kim, Y.-S. Chung, C.-K. Yoo, M.-G. Han, Genome-wide identification and characterization of point mutations in the SARS-CoV-2 genome, Osong Public Health Res. Perspect. 11 (3) (2020) 101.
[5] S. Weber, C.M. Ramirez, B. Weiser, H. Burger, W. Doerfler, Sars-cov-2 worldwide replication drives rapid rise and selection of mutations across the viral genome: a time-course study–potential challenge for vaccines and therapies, EMBO Mol. Med. 13 (6) (2021), e14062.
[6] P.R. Krause, T.R. Fleming, I.M. Longini, R. Peto, S. Briand, D.L. Heymann, V. Beral, M.D. Snape, H. Rees, A.-M. Ropero, et al., SARS-CoV-2 variants and vaccines, N. Engl. J. Med. 385 (2) (2021) 179–186.
[7] F. Touret, L. Luciani, C. Baronti, M. Cochin, J.-S. Driouich, M. Gilles, L. Thirion, A. Nougairede, X. de Lamballerie, Replicative fitness of a SARS-CoV-2 20i/501y. v1 variant from lineage b. 1.1. 7 in human reconstituted bronchial epithelium, Mbio 12 (4) (2021), e00850–21.
[8] A.K. Padhi, T. Tripathi, Can SARS-CoV-2 accumulate mutations in the s-protein to increase pathogenicity? ACS Pharmacol. Transl. Sci. 3 (5) (2020) 1023–1026.
[9] A.T. Chen, K. Altschuler, S.H. Zhan, Y.A. Chan, B.E. Deverman, COVID-19 cg enables SARS-CoV-2 mutation and lineage tracking by locations and dates of interest, eLife 10 (2021), e63409.
[10] A.K. Padhi, R. Shukla, P. Saudagar, T. Tripathi, High-throughput rational design of the remdesivir binding site in the RDRP of SARS-CoV-2: implications for potential resistance, Iscience 24 (1) (2021), 101992.
[11] S. Desai, S. Rashmi, A. Rane, B. Dharavath, A. Sawant, A. Dutt, An integrated approach to determine the abundance, mutation rate and phylogeny of the SARS-CoV-2 genome, Brief. Bioinform. 22 (2) (2021) 1065–1075.
[12] A.K. Padhi, J. Dandapat, P. Saudagar, V.N. Uversky, T. Tripathi, Interface-based design of the favipiravir-binding site in SARS-CoV-2 RNA-dependent RNA polymerase reveals mutations conferring resistance to chain termination, FEBS Lett. 595 (18) (2021) 2366–2382.
[13] M.T. Maurano, S. Ramaswami, P. Zappile, D. Dimartino, L. Boytard, A.M. Ribeiro-dos Santos, N.A. Vulpescu, G. Westby, G. Shen, X. Feng, et al., Sequencing identifies multiple early introductions of SARS-CoV-2 to the New York city region, Genome Res. 30 (12) (2020) 1781–1788.
[14] C. Bi, G. Ramos-Mandujano, Y. Tian, S. Hala, J. Xu, S. Mfarrej, C.R. Esteban, E. N. Delicado, F.S. Alofi, A. Khogeer, et al., Simultaneous detection and mutation surveillance of SARS-CoV-2 and multiple respiratory viruses by rapid field-deployable sequencing, Med 2 (6) (2021) 689–700.e4.
[15] S. Satarker, M. Nampoothiri, Structural proteins in severe acute respiratory syndrome coronavirus-2, Arch. Med. Res. 51 (6) (2020) 482–491.
[16] D. Wang, A. Jiang, J. Feng, G. Li, D. Guo, M. Sajid, K. Wu, Q. Zhang, Y. Ponty, S. Will, et al., The SARS-CoV-2 subgenome landscape and its novel regulatory features, Mol. Cell 81 (10) (2021) 2135–2147.
[17] S.M. Kasibhatla, M. Kinikar, S. Limaye, M.M. Kale, U. Kulkarni-Kale, Understanding evolution of SARS-CoV-2: a perspective from analysis of genetic diversity of RDRP gene, J. Med. Virol. 92 (10) (2020) 1932–1937.
[18] C.J. Michel, C. Mayer, O. Poch, J.D. Thompson, Characterization of accessory genes in coronavirus genomes, Virol. J. 17 (1) (2020) 1–13.

[19] S.J.R.d. Silva, C.T.A.d. Silva, R.P.G. Mendes, L. Pena, in: Role of nonstructural proteins in the pathogenesis of SARS-CoV-2 92 (9), 2020, pp. 1427–1429.
[20] H.S. Hillen, G. Kokic, L. Farnung, C. Dienemann, D. Tegunov, P. Cramer, Structure of replicating SARS-CoV-2 polymerase, Nature 584 (7819) (2020) 154–156.
[21] L.K. Clark, T.J. Green, C.M. Petit, Structure of nonstructural protein 1 from SARS-CoV-2, J. Virol. 95 (4) (2021) e02019–e02020.
[22] A. Shannon, N.T.-T. Le, B. Selisko, C. Eydoux, K. Alvarez, J.-C. Guillemot, E. Decroly, O. Peersen, F. Ferron, B. Canard, Remdesivir and SARS-CoV-2: structural requirements at both Nsp12 RDRP and Nsp14 exonuclease active-sites, Antivir. Res. 178 (2020), 104793.
[23] S. Duffy, Why are RNA virus mutation rates so damn high? PLoS Biol. 16 (8) (2018), e3000003.
[24] S.F. Elena, R. Sanjuán, Adaptive value of high mutation rates of RNA viruses: separating causes from consequences, J. Virol. 79 (18) (2005) 11555–11558.
[25] L. Yan, Y. Yang, M. Li, Y. Zhang, L. Zheng, J. Ge, Y.C. Huang, Z. Liu, T. Wang, S. Gao, et al., Coupling of n7-methyltransferase and 3`-5` exoribonuclease with SARS-CoV-2 polymerase reveals mechanisms for capping and proofreading, Cell 184 (13) (2021) 3474–3485.
[26] J. Chen, R. Wang, M. Wang, G.-W. Wei, Mutations strengthened SARS-CoV-2 infectivity, J. Mol. Biol. 432 (19) (2020) 5212–5226.
[27] D. Eskier, G. Karakulah, A. Suner, Y. Oktay, RDRP mutations are associated with SARS-CoV-2 genome evolution, PeerJ 8 (2020) e9587.
[28] A.M. Gupta, J. Chakrabarti, S. Mandal, Non-synonymous mutations of SARS-CoV-2 leads epitope loss and segregates its variants, Microbes Infect. 22 (10) (2020) 598–607.
[29] S.S. Hassan, P.P. Choudhury, B. Roy, SARS-CoV-2 envelope protein: non-synonymous mutations and its consequences, Genomics 112 (6) (2020) 3890–3892.
[30] E. Issa, G. Merhi, B. Panossian, T. Salloum, S. Tokajian, SARS-CoV-2 and Orf3a: nonsynonymous mutations, functional domains, and viral pathogenesis, mSystems 5 (3) (2020), e00266–20.
[31] M. Seyran, D. Pizzol, P. Adadi, T.M. El-Aziz, S.S. Hassan, A. Soares, R. Kandimalla, K. Lundstrom, M. Tambuwala, A.A. Aljabali, et al., Questions concerning the proximal origin of SARS-CoV-2, J. Med. Virol. 93 (3) (2021) 1204.
[32] K. Narayanan, C. Huang, S. Makino, Sars coronavirus accessory proteins, Virus Res. 133 (1) (2008) 113–121.
[33] S.S. Hassan, D. Attrish, S. Ghosh, P.P. Choudhury, V.N. Uversky, A.A. Aljabali, K. Lundstrom, B.D. Uhal, N. Rezaei, M. Seyran, et al., Notable sequence homology of the orf10 protein introspects the architecture of SARS-CoV-2, Int. J. Biol. Macromol. 181 (2021) 801–809.
[34] N.A. Schuster, Characterization and structural prediction of the putative orf10 protein in SARS-CoV-2, bioRxiv, 2021, 2020–10.
[35] N. Altincekic, S.M. Korn, N.S. Qureshi, M. Dujardin, M. Ninot-Pedrosa, R. Abele, M. J. Abi Saad, C. Alfano, F.C. Almeida, I. Alshamleh, et al., Large-scale recombinant production of the SARS-CoV-2 proteome for high-throughput and structural biology applications, Front. Mol. Biosci. 8 (2021) 89.
[36] D.E. Gordon, G.M. Jang, M. Bouhaddou, J. Xu, K. Obernier, K.M. White, M. J. O'Meara, V.V. Rezelj, J.Z. Guo, D.L. Swaney, et al., A sars-cov-2 protein interaction map reveals targets for drug repurposing, Nature 583 (7816) (2020) 459–468.
[37] E.L. Mena, C.J. Donahue, L.P. Vaites, J. Li, G. Rona, C. O'Leary, L. Lignitto, B. Miwatani-Minter, J.A. Paulo, A. Dhabaria, Orf10–cullin-2–zyg11b complex is not required for SARS-CoV-2 infection, Proc. Natl. Acad. Sci. 118 (17) (2021).
[38] J. Li, M. Guo, X. Tian, X. Wang, X. Yang, P. Wu, C. Liu, Z. Xiao, Y. Qu, Y. Yin, et al., Virus-host interactome and proteomic survey reveal potential virulence factors influencing SARS-CoV-2 pathogenesis, Med 2 (1) (2021) 99–112.
[39] K. Pancer, A. Milewska, K. Owczarek, A. Dabrowska, M. Kowalski, P.P. Łabaj, W. Branicki, M. Sanak, K. Pyrc, The SARS-CoV-2 Orf10 is not essential in vitro or in vivo in humans, PLoS Pathog. 16 (12) (2020), e1008959.
[40] D.-M. Yang, F.-C. Lin, P.-H. Tsai, Y. Chien, M.-L. Wang, Y.-P. Yang, T.-J. Chang, Pandemic analysis of infection and death correlated with genomic open reading frame 10 mutation in severe acute respiratory syndrome coronavirus 2 victims, J. Chin. Med. Assoc. 84 (5) (2021) 478–484.
[41] R. Cagliani, D. Forni, M. Clerici, M. Sironi, Coding potential and sequence conservation of SARS-CoV-2 and related animal viruses, Infect. Genet. Evol. 83 (2020), 104353.
[42] L. Käll, A. Krogh, E.L. Sonnhammer, A combined transmembrane topology and signal peptide prediction method, J. Mol. Biol. 338 ((5) (2004) 1027–1036.
[43] F. Madeira, Y.M. Park, J. Lee, N. Buso, T. Gur, N. Madhusoodanan, P. Basutkar, A. R. Tivey, S.C. Potter, R.D. Finn, et al., The embl-ebi search and sequence analysis tools apis in 2019, Nucleic Acids Res. 47 (W1) (2019) W636–W641.
[44] A. Drozdetskiy, C. Cole, J. Procter, G.J. Barton, Jpred4: a protein secondary structure prediction server, Nucleic Acids Res. 43 (W1) (2015) W389–W394.
[45] Z. Obradovic, K. Peng, S. Vucetic, P. Radivojac, A.K. Dunker, Exploiting heterogeneous sequence properties improves prediction of protein disorder, Proteins 61 (S7) (2005) 176–182.
[46] F. Meng, V.N. Uversky, L. Kurgan, Comprehensive review of methods for prediction of intrinsic disorder and its molecular functions, Cell. Mol. Life Sci. 74 (17) (2017) 3069–3090.
[47] Z.-L. Peng, L. Kurgan, Comprehensive comparative assessment of in-silico predictors of disordered regions, Curr. Protein Pept. Sci. 13 (1) (2012) 6–18.
[48] X. Fan, L. Kurgan, Accurate prediction of disorder in protein chains with a comprehensive and empirically designed consensus, J. Biomol. Struct. Dyn. 32 (3) (2014) 448–464.
[49] B.E. Pickett, E.L. Sadat, Y. Zhang, J.M. Noronha, R.B. Squires, V. Hunt, M. Liu, S. Kumar, S. Zaremba, Z. Gu, et al., Vipr: an open bioinformatics database and analysis resource for virology research, Nucleic Acids Res. 40 (D1) (2012) D593–D598.
[50] J. Bendl, J. Stourac, O. Salanda, A. Pavelka, E.D. Wieben, J. Zendulka, J. Brezovsky, J. Damborsky, Predictsnp: robust and accurate consensus classifier for prediction of disease-related mutations, PLoS computational biology 10 (1) (2014) e1003440.E. Capriotti, P. Fariselli, Phd-snpg: a webserver and lightweight tool for scoring single nucleotide variants, Nucleic Acids Res. 45 (W1) (2017) W247–W252.
[51] R. Henson, L. Cetto, The Matlab bioinformatics toolbox, in: Encyclopedia of Genetics, Genomics, Proteomics And Bioinformatics, 2004.
[52] J. Bendl, J. Stourac, O. Salanda, A. Pavelka, E.D. Wieben, J. Zendulka, J. Brezovsky, J. Damborsky, PredictSNP: robust and accurate consensus classifier for prediction of disease-related mutations, PLoS Comput. Biol. 10 (1) (2014), e1003440.
[53] S.S. Hassan, A.A. Aljabali, P.K. Panda, S. Ghosh, D. Attrish, P.P. Choudhury, M. Seyran, D. Pizzol, P. Adadi, T.M.Abd El-Aziz, A unique view of SARS-CoV-2 through the lens of orf8 protein, Comput. Biol. Med. 133 (2021), 104380.
[54] S.S. Hassan, P.P. Choudhury, B. Roy, S.S. Jana, Missense mutations in SARS-CoV-2 genomes from Indian patients, Genomics 112 (6) (2020) 4622–4627.
[55] B. Mészáros, G. Erdos, Z. Dosztányi, IUPred2a: context-dependent prediction of protein disorder as a function of redox state and protein binding, Nucleic Acids Res. 46 (W1) (2018) W329–W337.
[56] D. Szklarczyk, A. Franceschini, M. Kuhn, M. Simonovic, A. Roth, P. Minguez, T. Doerks, M. Stark, J. Muller, P. Bork, et al., The STRING database in 2011: functional interaction networks of proteins, globally integrated and scored, Nucleic Acids Res. 39 (suppl 1) (2010) D561–D568.
[57] P. Romero, Z. Obradovic, X. Li, E.C. Garner, C.J. Brown, A.K. Dunker, Sequence complexity of disordered protein, Proteins 42 (1) (2001) 38–48.
[58] K. Peng, S. Vucetic, P. Radivojac, C.J. Brown, A.K. Dunker, Z. Obradovic, Optimizing long intrinsic disorder predictors with protein evolutionary information, J. Bioinforma. Comput. Biol. 3 (01) (2005) 35–60.
[59] K. Peng, P. Radivojac, S. Vucetic, A.K. Dunker, Z. Obradovic, Length-dependent prediction of protein intrinsic disorder, BMC Bioinforma. 7 (1) (2006) 1–17.
[60] B. Xue, R.L. Dunbrack, R.W. Williams, A.K. Dunker, V.N. Uversky, PONDR-FIT: a meta-predictor of intrinsically disordered amino acids, Biochim. Biophys. Acta Protein Proteomics 1804 (4) (2010) 996–1010.
[61] K. Rajagopalan, S.M. Mooney, N. Parekh, R.H. Getzenberg, P. Kulkarni, A majority of the cancer/testis antigens are intrinsically disordered proteins, J. Cell. Biochem. 112 (11) (2011) 3256–3267.
[62] B. Mészáros, I. Simon, Z. Dosztányi, Prediction of protein binding regions in disordered proteins, PLoS Comput. Biol. 5 (5) (2009), e1000376.
[63] R. Oughtred, C. Stark, B.-J. Breitkreutz, J. Rust, L. Boucher, C. Chang, N. Kolas, L. O'Donnell, G. Leung, R. McAdam, et al., The biogrid interaction database: 2019 update, Nucleic Acids Res. 47 (D1) (2019) D529–D541.
[64] L.M. Iakoucheva, P. Radivojac, C.J. Brown, T.R. O'Connor, J.G. Sikes, Z. Obradovic, A.K. Dunker, The importance of intrinsic disorder for protein phosphorylation, Nucleic Acids Res. 32 (3) (2004) 1037–1049.
[65] V. Pejaver, W.-L. Hsu, F. Xin, A.K. Dunker, V.N. Uversky, P. Radivojac, The structural and functional signatures of proteins that undergo multiple events of post-translational modification, Protein Sci. 23 (8) (2014) 1077–1093.
[66] A.L. Darling, V.N. Uversky, Intrinsic disorder and posttranslational modifications: the darker side of the biological dark matter, Front. Genet. 9 (2018) 158.
[67] D. Haddad, S.E. John, A. Mohammad, M.M. Hammad, P. Hebbar, A. Channanath, R. Nizam, S. Al-Qabandi, A. Al Madhoun, A. Alshukry, H. Ali, T.A. Thanaraj, F. Al-Mulla, SARS-CoV-2: possible recombination and emergence of potentially more virulent strains, PLoS One 16 (5) (2021), e0251368.